



**HAL**  
open science

# Lyman- $\alpha$ emitters in the context of hierarchical galaxy formation: predictions for VLT/MUSE surveys

T. Garel, B. Guiderdoni, J. Blaizot

► **To cite this version:**

T. Garel, B. Guiderdoni, J. Blaizot. Lyman- $\alpha$  emitters in the context of hierarchical galaxy formation: predictions for VLT/MUSE surveys. *Monthly Notices of the Royal Astronomical Society*, 2016, 455, pp.3436-3452. 10.1093/mnras/stv2467 . insu-03710586

**HAL Id: insu-03710586**

**<https://insu.hal.science/insu-03710586>**

Submitted on 1 Jul 2022

**HAL** is a multi-disciplinary open access archive for the deposit and dissemination of scientific research documents, whether they are published or not. The documents may come from teaching and research institutions in France or abroad, or from public or private research centers.

L'archive ouverte pluridisciplinaire **HAL**, est destinée au dépôt et à la diffusion de documents scientifiques de niveau recherche, publiés ou non, émanant des établissements d'enseignement et de recherche français ou étrangers, des laboratoires publics ou privés.

# Lyman- $\alpha$ emitters in the context of hierarchical galaxy formation: predictions for VLT/MUSE surveys

T. Garel,<sup>1,2\*</sup> B. Guiderdoni<sup>2</sup> and J. Blaizot<sup>2</sup>

<sup>1</sup>Centre for Astrophysics and Supercomputing, Swinburne University of Technology, Hawthorn, Victoria 3122, Australia

<sup>2</sup>Centre de Recherche Astrophysique de Lyon, Université de Lyon, Université Lyon 1, CNRS, Observatoire de Lyon; 9 avenue Charles André, F-69561 Saint-Genis Laval Cedex, France

Accepted 2015 October 22. Received 2015 October 22; in original form 2015 January 28

## ABSTRACT

The VLT/Multi Unit Spectrograph Explorer (MUSE) integral-field spectrograph can detect Ly $\alpha$  emitters (LAE) in the redshift range  $2.8 \lesssim z \lesssim 6.7$  in a homogeneous way. Ongoing MUSE surveys will notably probe faint Ly $\alpha$  sources that are usually missed by current narrow-band surveys. We provide quantitative predictions for a typical wedding-cake observing strategy with MUSE based on mock catalogues generated with a semi-analytic model of galaxy formation coupled to numerical Ly $\alpha$  radiation transfer models in gas outflows. We expect  $\approx 1500$  bright LAEs ( $F_{\text{Ly}\alpha} \gtrsim 10^{-17}$  erg s $^{-1}$  cm $^{-2}$ ) in a typical shallow field (SF) survey carried over  $\approx 100$  arcmin $^2$ , and  $\approx 2000$  sources as faint as  $10^{-18}$  erg s $^{-1}$  cm $^{-2}$  in a medium-deep field (MDF) survey over 10 arcmin $^2$ . In a typical deep field (DF) survey of 1 arcmin $^2$ , we predict that  $\approx 500$  extremely faint LAEs ( $F_{\text{Ly}\alpha} \gtrsim 4 \times 10^{-19}$  erg s $^{-1}$  cm $^{-2}$ ) will be found. Our results suggest that faint Ly $\alpha$  sources contribute significantly to the cosmic Ly $\alpha$  luminosity and SFR budget. While the host haloes of bright LAEs at  $z \approx 3$  and 6 have descendants with median masses of  $2 \times 10^{12}$  and  $5 \times 10^{13}$  M $_{\odot}$ , respectively, the faintest sources detectable by MUSE at these redshifts are predicted to reside in haloes which evolve into typical sub-L\* and L\* galaxy haloes at  $z = 0$ . We expect typical DF and MDF surveys to uncover the building blocks of Milky Way-like objects, even probing the bulk of the stellar mass content of LAEs located in their progenitor haloes at  $z \approx 3$ .

**Key words:** methods: numerical – galaxies: evolution – galaxies: formation – galaxies: high-redshift.

## 1 INTRODUCTION

Since the late nineties, the Ly $\alpha$  emission line has become increasingly efficient at detecting high-redshift star-forming galaxies. Ly $\alpha$  emitters (LAE) are now commonly found up to a redshift of seven, allowing us to study the formation and evolution of galaxies in the early Universe. Most LAEs have been extensively probed in narrow-band (NB) imaging surveys (e.g. Hu, Cowie & McMahon 1998; Rhoads et al. 2000; Shimasaku et al. 2006; Ouchi et al. 2008), and blind spectroscopic searches have led to hundreds of detections, especially in the last years (Rauch et al. 2008; Blanc et al. 2011; Cassata et al. 2011). These observations have mainly put statistical constraints on the LAE population at  $F_{\text{Ly}\alpha} \gtrsim 10^{-17}$  erg s $^{-1}$  cm $^{-2}$  (e.g. Ly $\alpha$  luminosity functions and clustering) and they tend to show that LAEs are slightly less massive, bluer and more metal-poor than the other well-studied high-redshift galaxy population, the Lyman-break galaxies (LBG; Shapley et al. 2001, 2003; Pentericci et al.

2007; Bouwens et al. 2009). However, the existing Ly $\alpha$  data remains somewhat more inhomogeneous than that of dropout galaxies, due to the different selection methods used in various surveys, potential significant contamination and rather small statistics.

The acquisition of large, homogeneous, spectroscopic samples of Ly $\alpha$  emitting galaxies is one of the main objectives of the VLT Multi Unit Spectrograph Explorer (MUSE; Bacon et al. 2006) which started to operate in 2014. The MUSE integral-field spectrograph, which has a field-of-view of 1 arcmin $^2$ , will probe the Ly $\alpha$  emission line from  $z \approx 2.8$  to  $\approx 6.7$ . MUSE has been optimized for performing deep field observations, and it will thus enable to detect very faint LAEs at high redshift.

A few tens of objects have been observed previously at  $F_{\text{Ly}\alpha} \gtrsim 10^{-18}$  erg s $^{-1}$  cm $^{-2}$  (Rauch et al. 2008; Cassata et al. 2011; Dressler et al. 2015). MUSE is expected to dramatically increase the statistics at these fluxes, and furthermore explore an uncharted territory with LAEs as faint as  $\approx 4 \times 10^{-19}$  erg s $^{-1}$  cm $^{-2}$  (Bacon et al. 2010).

These unprecedentedly low Ly $\alpha$  detection limits will offer a glimpse of the population of dwarf star-forming galaxies in the early Universe, unveiling objects with star formation rates (SFRs)

\*E-mail: thibault.garel@univ-lyon1.fr

much lower than current LAE and LBG surveys. This will therefore provide fundamental knowledge on the properties of galaxies at high redshift that will put tight constraints on models of galaxy formation. As high-redshift sources are the building blocks of local galaxies in the hierarchical merging scenario, these faint LAEs are natural candidates to be the progenitors of local late-type galaxies. MUSE will help constrain the abundance of the population of faint galaxies and their contribution to the global SFR density from  $z \approx 3$  to  $\approx 7$ , allowing us to investigate the mass assembly of our Galaxy.

Besides, in order to help refine the observing strategy for MUSE surveys and interpret forthcoming data, it is essential to develop theoretical tools able to predict the expected number counts as a function of Ly $\alpha$  flux and redshift, and to quantify the effect of cosmic variance. Simple models have been developed in order to interpret the existing observational constraints at high-redshift. Using cosmological simulations, Nagamine et al. (2010) explore a stochastic scenario, in which galaxies undergo a Ly $\alpha$ -bright phase of finite duration, and adjust the Ly $\alpha$  luminosity functions at  $z \approx 3$ –6 assuming all Ly $\alpha$  photons can escape the galaxy. It is however well-known that interstellar/circumgalactic gas kinematics and distribution strongly affect the Ly $\alpha$  line profile and escape fraction ( $f_{\text{esc}}$ ; Neufeld 1990; Tenorio-Tagle et al. 1999; Mas-Hesse et al. 2003; Shapley et al. 2003; Steidel et al. 2010), so the complex radiative transfer (RT) of resonant Ly $\alpha$  photons must be accounted for. While Le Delliou et al. (2005) adopted a simple, constant  $f_{\text{esc}}$  model to match the Ly $\alpha$  LF (see also Dayal, Ferrara & Gallerani 2008; Nagamine et al. 2010), more refined models were investigated to describe  $f_{\text{esc}}$  for various interstellar medium configurations (slab geometry, clumpy dust distribution, static/outflow phases, etc.) using phenomenological recipes (e.g. Haiman & Spaans 1999; Kobayashi, Totani & Nagashima 2007; Dayal, Ferrara & Saro 2010; Kobayashi, Totani & Nagashima 2010; Dayal, Maselli & Ferrara 2011; Shimizu, Yoshida & Okamoto 2011).

Yet, the accurate treatment of the Ly $\alpha$  RT in galaxies requires numerical Monte Carlo calculations, that can be performed as a post-processing step of hydrodynamical simulation runs (Laursen, Sommer-Larsen & Andersen 2009; Zheng et al. 2010; Verhamme et al. 2012; Yajima et al. 2012a). These are highly (CPU-)time-consuming and a trade-off must be found between the size of the galaxy sample and the need for sufficient spatial resolution at the galaxy scale, preventing the use of Ly $\alpha$  RT algorithms on to statistical galaxy samples in high-resolution simulations. To bypass this issue, semi-analytic models or hydrodynamical simulations can be coupled with results of Ly $\alpha$  RT experiments in idealized geometries, like a slab-like configuration (Forero-Romero et al. 2011), or the so-called shell model (Garel et al. 2012; Orsi, Lacey & Baugh 2012). This method provides a very suitable alternative due to much smaller computing time requirements, although their description of galaxies is more idealized than in high-resolution hydrodynamical simulations.

Here, we use the model of Garel et al. (2015) which couples the GALICS hybrid of model of galaxy formation (Hatton et al. 2003) with a grid of numerical Ly $\alpha$  RT calculations through gas outflows (Schaerer et al. 2011). Using this model, we create mock lightcones to make quantitative predictions for typical MUSE surveys of LAEs, and intend to assess the role of these objects in the hierarchical scenario of galaxy formation. Our paper is laid out as follows. In Section 2, we describe our model and the mock catalogues of LAEs. Section 3 gives a brief overview of the existing data sets of LAEs. In Section 4, we present our predictions in terms of number counts, Ly $\alpha$  luminosity and SFR budget that can be probed by typical MUSE surveys. In Section 5, we investigate the descendant/progenitor

link between high redshift LAEs and present-day objects, and discuss our results on Section 6. Finally, we give a summary in Section 7.

Throughout this paper, we assume the following set of cosmological parameters:  $h = H_0/(100 \text{ km s}^{-1} \text{ Mpc}^{-1}) = 0.70$ ,  $\Omega_\Lambda = 0.72$ ,  $\Omega_m = 0.28$ ,  $\Omega_b = 0.046$ , and  $\sigma_8 = 0.82$ , consistent with the WMAP-5 results (Komatsu et al. 2009). All magnitudes are expressed in the AB system.

## 2 SEMI-ANALYTIC MODELLING AND MOCK CATALOGUES

In this paper, we use mock catalogues of Ly $\alpha$ -emitting galaxies computed with the model set out in Garel et al. (2015, see also Garel et al. 2012) which combines a hybrid approach for the formation of galaxies in the cosmological context with a simple model of Ly $\alpha$  emission and transfer.

We describe the formation and evolution of galaxies with GALICS (*GALaxies In Cosmological Simulations*; Hatton et al. 2003). The GALICS hybrid model includes (i) the hierarchical growth of dark matter (DM) structures described by an  $N$ -body cosmological simulation, and (ii) semi-analytic prescriptions to model the evolution of the baryonic component within virialized DM haloes. The GALICS version that we use is based on the original model of Hatton et al. (2003) and subsequent updates presented in Blaizot et al. (2004), Lanzoni et al. (2005), and Cattaneo et al. (2006, see also Garel et al. 2012, 2015). The output of GALICS is combined in post-processing with a *shell* model (Verhamme et al. 2008) which describes the RT of Ly $\alpha$  photons through thin expanding shells of hydrogen gas homogeneously mixed with dust, used as a proxy for outflows triggered by supernovae. Below, we outline the main features of our model.

### 2.1 Cosmological $N$ -body simulation

Our  $N$ -body simulation has been run with GADGET (Springel 2005) using  $1024^3$  DM particles in a cubic periodic (comoving) volume of  $100 h^{-1}$  Mpc on a side. We assume a standard  $\Lambda$  cold dark matter (CDM) *concordance* cosmology in agreement with the WMAP-5 data release (Komatsu et al. 2009), which parameter values are given in Section 1. Halo identification is performed with a Friends-of-Friends algorithm (FOF; Davis et al. 1985) and we follow Tweed et al. (2009) to compute the merging histories of the DM haloes. The FOF links together groups of particles with overdensity of  $\sim 200$  times the mean density (which translates into a linking-length  $b$  of 0.2). Bound groups of  $\geq 20$  particles are then identified as haloes (see Hatton et al. 2003, for more details), hence the minimum halo mass we can resolve in our simulation is  $M_{\text{halo}}^{\text{min}} = 2 \times 10^9 M_\odot$ .

### 2.2 Baryonic prescriptions

In GALICS, galaxies are evolved through the DM halo merger trees using physically motivated and phenomenological semi-analytic prescriptions. We refer to Hatton et al. (2003) for a more complete description of the physical recipes and free parameters implemented in GALICS. Below, we only highlight the main ingredients as well as the departures from the original version.

In the original version of Hatton et al. (2003), a mass of hot gas  $M_{\text{hot}}$  was assigned to each DM halo when first identified, consistently with the primordial baryonic fraction (i.e.  $M_{\text{hot}} = \Omega_b/\Omega_m M_{\text{halo}}$ ). As the DM halo subsequently accreted mass, the hot gas reservoir was increased accordingly. At each timestep,

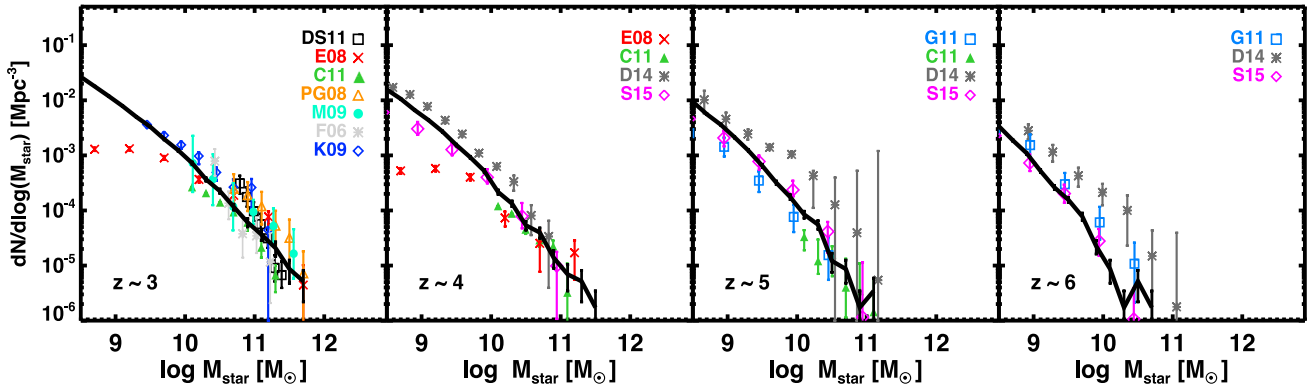


**Figure 1.** SMF at  $z \approx 3, 4, 5,$  and  $6$ . The solid black line with Poisson error bars corresponds to our model and the symbols are observational estimates (converted to our IMF) from Domínguez Sánchez et al. (2011, DS11), Elsner, Feulner & Hopp (2008, E08), Caputi et al. (2011, C11), Pérez-González et al. (2008, PG08), Marchesini et al. (2009, M09), Fontana et al. (2006, F06), Kajisawa et al. (2009, K09), González et al. (2011, G11), Duncan et al. (2014, D14), and Song et al. (2015, S15).

the hot gas was able to cool and form stars at the centre of the DM halo. This scheme was replaced in Cattaneo et al. (2006) by a bimodal mode of accretion in high-redshift galaxies (e.g. Birnboim & Dekel 2003; Ocvirk, Pichon & Teyssier 2008; Dekel et al. 2009). In this scenario, gas from the intergalactic medium (IGM) is shock-heated to the virial temperature in massive haloes, while cold gas can accrete along filaments at a rate set by the free-fall time below a critical halo mass set to  $10^{12} M_{\odot}$  at  $z = 3$ .

Unlike Hatton et al. (2003) who inferred the SFR directly from the mass of cold gas of the galaxy,  $M_{\text{cold}}$ , we have now implemented the Kennicutt–Schmidt law which computes the SFR surface density from the cold gas mass surface density:  $\Sigma_{\text{SFR}} = \epsilon \Sigma_{\text{cold}}^{1.4}$ . Here,  $\epsilon = 1$  gives the  $z=0$  normalization of Kennicutt (1998) in code units. As discussed in Garel et al. (2015), we require  $\epsilon = 5$  to reproduce observational constraints (i.e. luminosity functions) at the redshifts we are focusing on in this study, namely  $z \gtrsim 3$ . Newly formed stars are distributed according to the Kennicutt (1983) initial mass function (IMF) and their evolution is followed over substeps of 1 Myr.

We describe metal enrichment of the interstellar medium and supernovae feedback in a similar fashion as Hatton et al. (2003). Following Silk (2003), the gas ejection rate is proportional to  $\alpha_{\text{SN}} \text{SFR} / v_{\text{esc}}^2$ , where  $v_{\text{esc}}$  is the escape velocity and  $\alpha_{\text{SN}}$  is the feedback efficiency, set to 0.2 as in Cattaneo et al. (2006). The ejected (cold gas and metals) material can start being re-accreted at a constant rate through a galactic fountain after a time  $\tau_{\text{delay}}$  (set to half a halo dynamical time).

When two DM haloes merge, the galaxies they host are placed in the descendant halo. As we do not follow substructures, we decide that a satellite can either merge with the central galaxy over a free-fall time,<sup>1</sup> or it may collide with another satellite (satellite–satellite encounters), following the procedure described in Hatton et al. (2003, section 5).

The spectral energy distributions (SEDs) are computed from the star formation histories of galaxies using the STARDUST libraries (Devriendt, Guiderdoni & Sadat 1999) for a Kennicutt IMF. The effect of dust attenuation is given by equation 3 of Garel et al.

(2012) assuming a spherical geometry, consistent with the shell approximation described in the next paragraphs.

### 2.3 Model calibration and comparison to data

In Garel et al. (2015), our model was adjusted against observational constraints by choosing a set of reasonable model parameter values able to reproduce the luminosity functions of LBGs and LAEs at  $3 \lesssim z \lesssim 7$ . The UV luminosity function is a major constraint at high redshift and it is now reasonably well measured at  $z \approx 3$ – $7$  (e.g. Sawicki & Thompson 2006; Reddy et al. 2008; Bouwens et al. 2015). It traces the SFR of galaxies over a time-scale of  $\approx 100$  Myr (modulo the effect of dust) and our model can reproduce it at various redshifts (see section 3.1 in Garel et al. 2015). Here, we show in addition the stellar mass functions (SMF) from our model and compare them to observational estimates. As can be seen on Fig. 1, the predicted  $M_{\text{star}}$  distributions are in good agreement with the observations, considering the large scatter between the different estimates. The best match is obtained when comparing with the recent CANDELS data from Song et al. (2015) at  $z \approx 4, 5,$  and  $6$ . In Fig. 2, we explore the positive correlation between stellar mass and SFR at high redshifts. Here, we use three different cuts in absolute UV magnitude,  $M_{1500} = -19, -20,$  and  $-21$ , to try to mimic the observational selection of galaxies. We find a reasonable agreement between the model and the observational estimates, and this result appears to be weakly sensitive to the value of our UV magnitude cut.

It is important to stress that the derivation of physical quantities such as stellar masses and SFRs is subject to large uncertainties not always reflected by the error bars of data points in Figs 1 and 2, such as SED modelling assumptions, dust correction, or photometric redshift errors (e.g. Marchesini et al. 2009; Wilkins et al. 2012; Schaerer, de Barros & Sklias 2013; Stark et al. 2013). None the less, our model appears well calibrated against existing observations describing the build-up of galaxies at high redshift.

### 2.4 Emission and RT of the Ly $\alpha$ line

Under the case B approximation (Osterbrock & Ferland 2006), the Ly $\alpha$  emission line is powered by the reprocessing of two-thirds of the ionizing photons through a radiative cascade in the H II regions. The intrinsic Ly $\alpha$  luminosity is thus given by  $L_{\text{Ly}\alpha}^{\text{intr}} = \frac{2}{3} Q(H) \frac{h\nu c}{\lambda_{\alpha}}$ , where  $Q(H)$  is the production rate of hydrogen-ionizing photons

<sup>1</sup> Whereas the dynamical friction time was used in the original version of Hatton et al. (2003), we now merge satellites with central galaxies over a free-fall time to be consistent with the cold filamentary accretion mode.

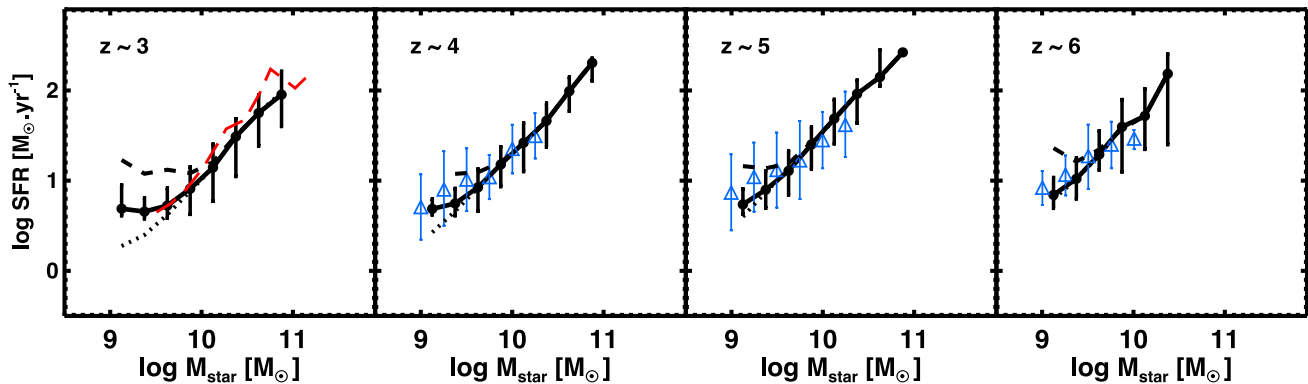


**Figure 2.** Relation between stellar mass ( $M_{\text{star}}$ ) and SFR at  $z \approx 3, 4, 5,$  and  $6$ . In black, we show the median SFR per bin of stellar mass along with the 10th–90th percentiles for galaxies with  $10^9 < (M_{\text{star}}/M_{\odot}) < 10^{11}$ . The dotted, solid, and dashed curves correspond to UV magnitude cuts of  $M_{1500} < -19$ ,  $M_{1500} < -20$ , and  $M_{1500} < -21$ , respectively. The red dashed line and the blue triangles correspond to the data from Kajisawa et al. (2010) and Salmon et al. (2015), respectively.

computed from the SEDs,  $\lambda_{\alpha} = 1215.67 \text{ \AA}$  is the Ly $\alpha$  wavelength at line centre,  $c$  is the speed of light,  $h_p$  the Planck constant. The intrinsic Ly $\alpha$  line is described by a Gaussian centred on  $\lambda_{\alpha}$  with a width given by the rotational velocity of the emission sources in the galaxy (see section 3.1 in Garel et al. 2012).

To account for the Ly $\alpha$  radiation transfer (RT) and dust extinction, we compute the escape of Ly $\alpha$  photons through galactic outflows. To do so, we combine the output of GALICS with the grid of Ly $\alpha$  RT models in spherical expanding shells presented in Schaerer et al. (2011). In these simulations, run with a 3D Monte Carlo code (MCLya; Verhamme, Schaerer & Maselli 2006), the thin spherical expanding shells of gas and dust are characterized by four parameters: the expansion velocity, the gas column density, the internal velocity dispersion, and the dust opacity. These parameters are estimated for each galaxy using simple scaling arguments connected to the output of GALICS as described in section 3.2.2 of Garel et al. (2012) and section 2 of Garel et al. (2015). We then compute the Ly $\alpha$  escape fraction by interpolating the shell parameters predicted by GALICS on to the MCLya grid to obtain the *observed* Ly $\alpha$  luminosity,  $L_{\text{Ly}\alpha}$ , and Ly $\alpha$  flux,  $F_{\text{Ly}\alpha} = L_{\text{Ly}\alpha}/(4\pi d_L^2(z))$  where  $d_L(z)$  is the luminosity distance at redshift  $z$ .

The above escape fraction only accounts for internal attenuation of Ly $\alpha$  photons (i.e. dust absorption in the shell). Nevertheless, interactions with H I gas along the line of sight may affect the blue side of the Ly $\alpha$  line, and then reduce the transmitted Ly $\alpha$  flux, especially at the highest redshifts. We have tested the effect of IGM on the Ly $\alpha$  lines using the prescriptions of Madau (1995) and Inoue et al. (2014) which compute the mean Ly $\alpha$  transmission from observational statistics of intergalactic absorbers. In our model, the Ly $\alpha$  lines are Doppler-shifted away from line centre due to RT in the shell, such that most photons emerging from our galaxies have  $\lambda > 1215.67 \text{ \AA}$  in the rest-frame of the source. The intervening neutral gas is transparent to these photons, and we find that the IGM has no noticeable impact on our Ly $\alpha$  fluxes even at  $z \approx 7$  (see section 3.2 of Garel et al. 2015 and section 4.4 of Garel et al. 2012 for more details). This modelling of the effect of IGM remains somehow crude, and a more realistic scenario would require a detailed description of the gas distribution, kinematics, or ionization state, which is beyond the capabilities of our semi-analytic approach. We note that the H I opacity may also affect the red side of the Ly $\alpha$  line due to peculiar gas motions in the surroundings of galaxies (e.g. infalls), or strong damping wings in a highly neutral Universe (i.e. before reionization is complete), which can thus reduce the overall transmitted

Ly $\alpha$  fluxes (e.g. Dijkstra, Lidz & Wyithe 2007; Iliev et al. 2008; Dayal et al. 2011; Laursen, Sommer-Larsen & Razoumov 2011; Jensen et al. 2013). We also note that faint LAEs might be more strongly attenuated than bright LAEs in inhomogeneously ionized IGM models at  $z > 6$  since bright sources are thought to sit in larger H II bubbles at the EoR, which may flatten the Ly $\alpha$  LF towards faint luminosities (Furlanetto, Zaldarriaga & Hernquist 2006; McQuinn et al. 2007).

## 2.5 Mass resolution of the simulation

MUSE is expected to carry out very deep Ly $\alpha$  observations, down to  $F_{\text{Ly}\alpha}^{\text{limit}} \approx 4 \times 10^{-19} \text{ erg s}^{-1} \text{ cm}^{-2}$ . In order to make reliable statistical predictions, we want to ensure that we have sufficient mass resolution to produce complete samples of LAEs with  $F_{\text{Ly}\alpha} \geq F_{\text{Ly}\alpha}^{\text{limit}}$ . In Fig. 3, we show the predicted intrinsic Ly $\alpha$  luminosity/flux of galaxies at  $z = 3$  (top panel) and  $z = 6$  (bottom panel) as a function of the mass of their host halo. The vertical line illustrates the halo mass-resolution limit of our simulation,  $M_{\text{halo}}^{\text{min}}$ . Galaxies can thus only form in haloes more massive than  $M_{\text{halo}}^{\text{min}}$ . For a given halo mass, galaxies can span a wide range of properties, i.e. stellar mass or Ly $\alpha$  emission, depending on their own accretion and star formation history. Hence, it is not straightforward to assess the galaxy mass or Ly $\alpha$  luminosity resolution limit. For the purpose of this paper, we consider the brightest intrinsic Ly $\alpha$  luminosity displayed by galaxies residing in the least massive haloes as a proxy for the Ly $\alpha$  luminosity resolution limit. From Fig. 3, we find this value to be  $\approx 2 \times 10^{40} \text{ erg s}^{-1}$  at  $z = 3$  and  $\approx 7 \times 10^{40} \text{ erg s}^{-1}$  at  $z = 6$ , corresponding approximately to the same Ly $\alpha$  flux of  $\approx 2 \times 10^{-19} \text{ erg s}^{-1} \text{ cm}^{-2}$  at both redshifts. Thus, we expect our samples of mock LAEs to be statistically complete for this current study.

In addition, we note that gas accretion can be suppressed within low-mass DM haloes as a result of photoheating of the IGM by a UV background during reionization (e.g. Efstathiou 1992). Using high-resolution hydrodynamic simulations, Okamoto, Gao & Theuns (2008) have shown that this effect becomes significant for haloes below a characteristic mass,  $M_C(z)$ .  $M_C(z) \approx 10^9$  and  $M_C(z) \approx 2 \times 10^8 M_{\odot}$  at  $z = 3$  and  $6$ , respectively. These values are below the minimum halo mass we can resolve in our simulation, so we assume that photoheating of the IGM would have a negligible impact on the baryonic content of our haloes, and we do not take it into account in our model.

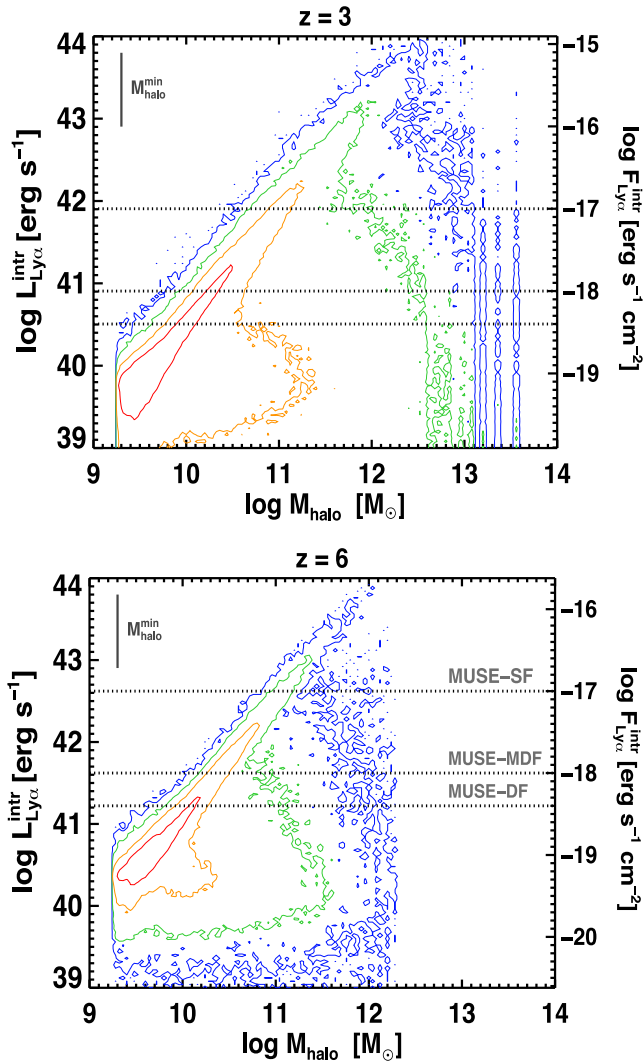


**Figure 3.** Intrinsic Ly $\alpha$  luminosity versus halo mass at  $z = 3$  (top panel) and  $z = 6$  (bottom panel). Contours show the number distribution of galaxies in the model. The vertical line in the top-left corner illustrates the halo mass resolution limit of the simulation ( $M_{\text{halo}}^{\text{min}} = 2 \times 10^9 M_{\odot}$ ). The dotted lines correspond to the Ly $\alpha$  flux limits of typical MUSE SF, MDF and DF surveys. The brightest Ly $\alpha$ -emitting galaxies residing in the least massive DM haloes in our model have an approximate intrinsic Ly $\alpha$  luminosity of  $2 \times 10^{40}$  erg s $^{-1}$  and  $7 \times 10^{40}$  erg s $^{-1}$  at  $z = 3$  and  $6$ , respectively (namely, a Ly $\alpha$  flux of  $\approx 2 \times 10^{-19}$  erg s $^{-1}$  cm $^{-2}$  at both redshifts). We consider that the sample of Ly $\alpha$ -emitting galaxies is complete above these values.

## 2.6 Mock catalogues

In order to produce mock observations easily comparable to real surveys, we convert the output of our semi-analytic model into lightcones with the MOMAF tool (*Mock Map Facility*; Blaizot et al. 2005). MOMAF performs the (random) tiling of the simulation box snapshots and computes the apparent properties of galaxies in a cone-like geometry. Thus, in addition to the physical properties of galaxies predicted by GALICS (SFRs, stellar masses, host halo masses, metallicity, gas content, etc), MOMAF provides an extra set of *observables*: apparent redshifts/positions/velocities/sizes, and Ly $\alpha$  fluxes.

In this paper, we assume an observing strategy with MUSE which consists of three typical surveys: a deep field (DF), a medium-deep field (MDF), and a shallow field (SF) survey that reach Ly $\alpha$  fluxes

of  $4 \times 10^{-19}$ ,  $10^{-18}$ , and  $10^{-17}$  erg s $^{-1}$  cm $^{-2}$ , respectively, corresponding approximately to 1, 10, and 80 h exposure $^{-1}$  (Bacon et al. 2010). We consider the DF, MDF, and SF surveys to cover a sky area of 1, 10, 100 arcmin $^2$ , respectively.

To assess the variance on the number counts, we generate a large number of each set of lightcones filled with mock galaxies in the redshift range where Ly $\alpha$  can be probed by MUSE ( $2.8 \lesssim z \lesssim 6.7$ ). We note that the effect of cosmic variance is inevitably underestimated here because we miss the fluctuations on the very large scales due to the finite comoving volume of our simulation box ( $\approx 3 \times 10^6$  Mpc $^3$ ).

## 3 REVIEW OF THE LITERATURE

In Fig. 4, we show LAE number counts reported by previous surveys at various redshifts in terms of LAE number density per unit redshift in four redshift intervals, i.e.  $2.8 < z < 4$ ,  $4 < z < 5$ ,  $5 < z < 6$ , and  $6 < z < 6.7$ . The flux limits of typical MUSE DF, MDF, and SF surveys are illustrated by arrows.

With a DF survey, MUSE could collect a sample of extremely faint galaxies, with a Ly $\alpha$  flux limit of  $4 \times 10^{-19}$  erg s $^{-1}$  cm $^{-2}$  in about 80 h over 1 arcmin $^2$ . Similar Ly $\alpha$  fluxes have already been reached by Santos (2004) in a spectroscopic blind survey using the strong lensing technique, but they only discovered a handful of objects at  $z = 4-6$ . A few years ago, Rauch et al. (2008) found 27 LAEs as part of a 92-h long-slit spectroscopy search with FORS2 at  $z \approx 3$ , which translates into a number density of objects at  $F_{\text{Ly}\alpha} \gtrsim 10^{-18}$  erg s $^{-1}$  cm $^{-2}$  as high as  $\approx 100$  LAE per arcmin $^2$  per unit redshift. Although the faintest source reported by Rauch et al. (2008) has a flux of  $\approx 7 \times 10^{-19}$  erg s $^{-1}$  cm $^{-2}$ , their distribution starts to flatten at  $\approx 10^{-18}$  erg s $^{-1}$  cm $^{-2}$ , probably due to incompleteness issues.

The Ly $\alpha$  detection limit of a MUSE MDF survey ( $F_{\text{Ly}\alpha} \approx 10^{-18}$  erg s $^{-1}$  cm $^{-2}$ ) will be comparable to the VVDS Ultra-Deep survey ( $2 \lesssim z \lesssim 6.6$ ; Cassata et al. 2011) and slightly deeper than the spectroscopic sample of Dressler et al. (2015) at  $z \approx 5.7$ . We show in Fig. 4 the number density of Ly $\alpha$  sources at  $2.8 \lesssim z \lesssim 4$  and  $4 \lesssim z \lesssim 5$  from the VVDS Ultra-Deep survey (serendipitous), including the slit losses  $\times 1.8$  flux correction quoted by Cassata et al. (2011). We note that the number counts at  $z = 2.8-4$  seem slightly less than those reported by Rauch et al. (2008), although the two measurements roughly remain in the (Poisson) error bars of one another. Also, while the detection limit of the VVDS Ultra-Deep survey is  $\approx 1.5 \times 10^{-18}$  erg s $^{-1}$  cm $^{-2}$ , the  $\approx 100$  per cent completeness level is reached at about  $F_{\text{Ly}\alpha} = 4-7 \times 10^{-18}$  erg s $^{-1}$  cm $^{-2}$  (see fig. 9 in Cassata et al. 2011) so their actual surface density of LAEs should be larger than what is shown in Fig. 4 at fainter fluxes. Furthermore, the volumes probed by these two surveys are rather small, so part of the difference may be due to cosmic variance effects.

At  $z \approx 6$ , the abundance of faint LAEs has recently been investigated by Dressler et al. (2015) using high-resolution IMACS observations, as a follow-up of a previous survey (Dressler et al. 2011). Targeting 110 out of their 210 LAE candidates, Dressler et al. (2015) spectroscopically confirmed about one-third of the sources as genuine high-redshift LAEs. Extrapolating this confirmation rate to the whole sample of candidates, the surface density of LAEs with  $F_{\text{Ly}\alpha} \gtrsim 2 \times 10^{-18}$  erg s $^{-1}$  cm $^{-2}$  is  $\approx 6$  arcmin $^{-2}$  per unit redshift, and  $\approx 10$  arcmin $^{-2}$  per unit redshift once corrected for incompleteness (Dressler, private communication), which

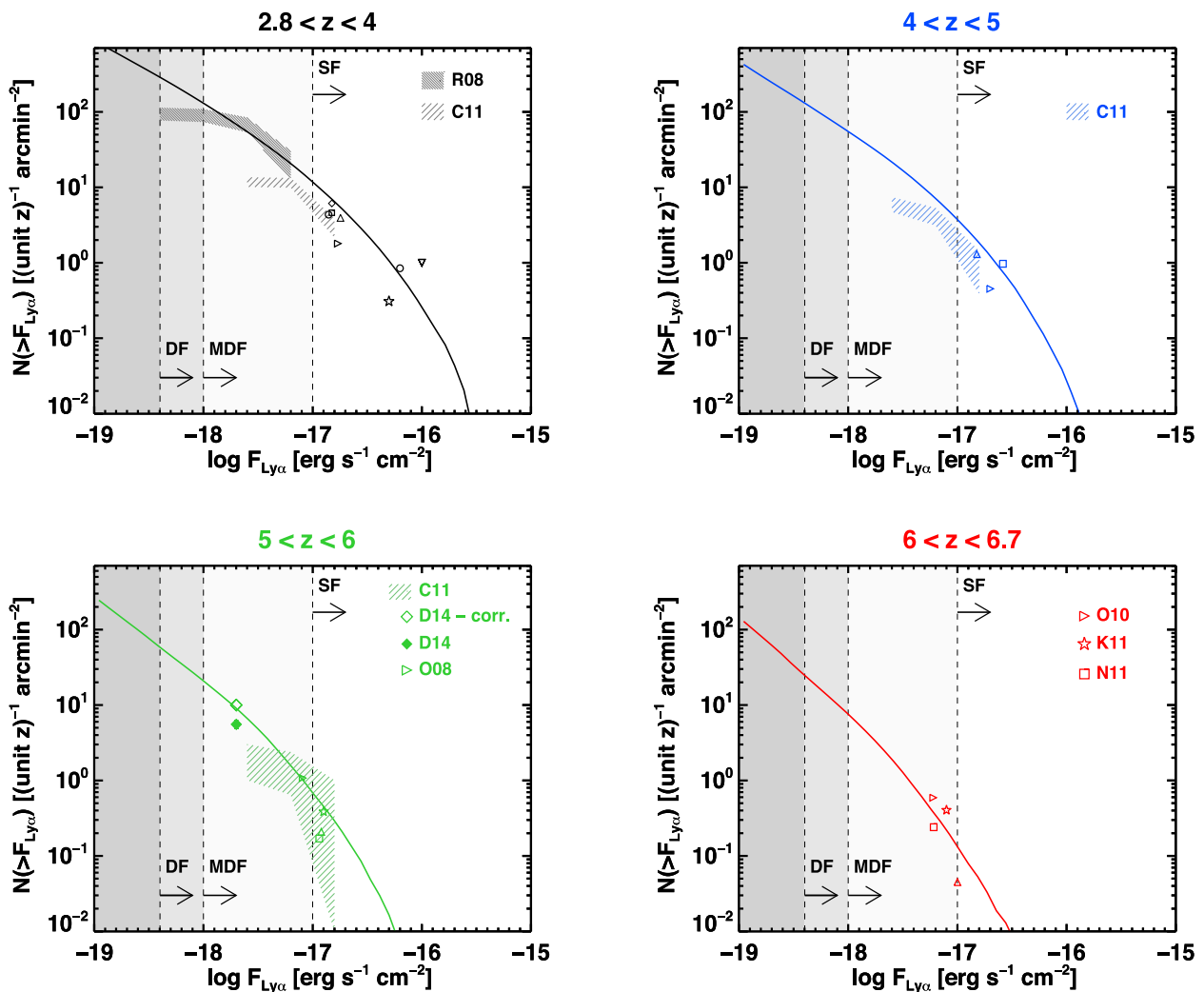


**Figure 4.** Mean number count predictions (curves) at four different redshifts:  $2.8 < z < 4$ ,  $4 < z < 5$ ,  $5 < z < 6$ , and  $6 < z < 6.7$ . The arrows show the limiting fluxes for typical MUSE Deep, Medium-Deep, and Shallow field surveys (DF, MDF and SF, respectively). The dashed areas encompass the error bars (Poisson statistics) of the data of Rauch et al. (2008, R11) and the VVDS Ultra-Deep serendipitous detections of Cassata et al. (2011, C11). The filled (empty) green diamond correspond to the number counts of Dressler et al. (2015) without (with) incompleteness correction (D14). The faint data ( $F_{\text{Ly}\alpha} \lesssim 10^{-17} \text{ erg s}^{-1} \text{ cm}^{-2}$ ) of Ouchi et al. (2008), Ouchi et al. (2010), Nakamura et al. (2011), and Kashikawa et al. (2011) are labelled O08, O10, N11 and K11, respectively. For the sake of clarity, the references for shallower surveys ( $F_{\text{Ly}\alpha} \gtrsim 10^{-17} \text{ erg s}^{-1} \text{ cm}^{-2}$ ) are not shown in the legend: van Breukelen, Jarvis & Venemans (2005, black circle), Yamada et al. (2012, black upward triangle), Hayashino et al. (2004, black diamond), Ouchi et al. (2008, black rightward triangle), Kudritzki et al. (2000, black downward triangle), Gronwall et al. (2007, black square), Blanc et al. (2011, black star), Hu et al. (1998, blue upward triangle), Rhoads et al. (2000, blue square), Malhotra & Rhoads (2004, blue rightward triangle), Murayama et al. (2007, green square), Kashikawa et al. (2011, green and red star) and Hu et al. (2010, green and red upward triangle). Unless stated otherwise, the data points plotted here correspond to the number of detections at the flux limit of a given survey, which may not be the limit of completeness.

suggests a very steep faint end slope of the Ly $\alpha$  luminosity function at  $z = 5.7$ .

The detection limit of a SF survey would be of the same order of magnitude as most existing Ly $\alpha$  data sets ( $F_{\text{Ly}\alpha}^{\text{limit}} \approx 10^{-17} \text{ erg s}^{-1} \text{ cm}^{-2}$ ), which sample the bright end of the Ly $\alpha$  LF, i.e.  $L_{\text{Ly}\alpha} \gtrsim 1\text{--}5 \times 10^{42} \text{ erg s}^{-1}$  at  $z = 3\text{--}6$ . Wide-field NB surveys usually span a large area on the sky allowing us to obtain large samples of candidates within large volumes (up to a few  $\sim 10^6 \text{ Mpc}^3$ ; Ouchi et al. 2008; Yamada et al. 2012) and to minimize the effect of cosmic variance. They nevertheless can only select LAEs in a rather restricted redshift window ( $\Delta z \lesssim 0.1$ ), and usually necessitate extensive amounts of telescope time for spectroscopic follow-up observations, required to remove low-redshift interlopers. Alternatively, blind spectroscopic surveys can easily detect line emitters

over a wider redshift range, but they usually cannot probe large volumes due to the small area sampled by the slit ( $\sim 7 \times 10^4 \text{ Mpc}^3$ ; Sawicki et al. 2008), or small IFUs field-of-view ( $\sim 10^4 \text{ Mpc}^3$ ; van Breukelen et al. 2005). Yet the Hobby-Eberly Telescope Dark Energy Experiment (HETDEX; Hill et al. 2008), a blind spectroscopic survey making use of the wide field-of-view VIRUS integral field spectrograph, is expected to detect up to one million bright LAEs ( $F_{\text{Ly}\alpha} \gtrsim 3.5 \times 10^{-17} \text{ erg s}^{-1} \text{ cm}^{-2}$ ) over a  $60 \text{ deg}^2$  sky area between  $z \approx 1.9$  and 3.8, which corresponds to a volume of almost  $9 \text{ Gpc}^3$ . The HETDEX survey will take years to complete, but first observations of LAEs have already been released as part of the pilot survey (e.g. Blanc et al. 2011). Despite the much smaller area covered by a typical MUSE SF survey ( $\approx 100 \text{ arcmin}^2$ ), it will be very complementary to HETDEX, as it will be slightly deeper,

able to probe LAEs at much higher redshift and at higher spectral resolution.

Our number count predictions, represented by the curves in Fig. 4, are computed over the full sample of objects at each timestep in our simulation, using mock lightcones of  $1 \times 1 \text{ deg}^2$  which roughly corresponds to the angular size of our  $100h^{-1} \text{ Mpc}$  box at  $z \sim 3-6$ . They are in very good agreement with the faint LAE number counts ( $F_{\text{Ly}\alpha} \gtrsim 10^{-18} \text{ erg s}^{-1} \text{ cm}^{-2}$ ) reported by Rauch et al. (2008) at  $z \approx 3$  and Dressler et al. (2015) at  $z \approx 5.7$ . At  $F_{\text{Ly}\alpha} \gtrsim 3 \times 10^{-18} \text{ erg s}^{-1} \text{ cm}^{-2}$ , they are slightly higher than the projected densities of serendipitous LAEs measured by Cassata et al. (2011) in the VVDS Ultra-Deep survey at  $z \lesssim 5$ , albeit the agreement is reasonable at  $z = 5-6$ . Our model roughly matches number counts from shallower observations shown as symbols in Fig. 4. These correspond to the number of detections at the flux limit of each given survey, which may not be the limit of completeness. A more reliable comparison of our model with observed bright LAE abundances can be found in fig. 2 of Garel et al. (2015) where we plot the predicted luminosity functions against observed ones from  $z \approx 3-7$ . They reasonably agree over this redshift range but scatter remains in the  $\text{Ly}\alpha$  LF data, and we note that our model better matches the higher (lower) end of the envelope of data points at  $z \approx 3$  ( $z \approx 6$ ).

#### 4 MODEL PREDICTIONS

In this section, we present the predicted number counts of  $\text{Ly}\alpha$ -emitting galaxies for each typical MUSE survey, and the contri-

bution of these sources to the cosmic  $\text{Ly}\alpha$  luminosity density and cosmic SFR density as a function redshift.

##### 4.1 Predicted number counts for typical muse surveys

In Fig. 5, we show the redshift distributions that we predict for the three typical surveys we consider in the paper. The redshift range is set by the wavelength range for which MUSE will be able to probe  $\text{Ly}\alpha$  line emitters, i.e. from  $z \approx 2.8$  to  $\approx 6.7$ . The histograms in Fig. 5 give the mean expected number of objects as a function of redshift, and the shaded grey areas correspond to the standard deviation (that includes cosmic variance) computed over larger number of realizations of each field.

In Table 1, we present the predicted mean number counts with the associated standard deviations and the median counts, including the 10/90th percentiles. We predict that MUSE would detect as many as  $\approx 500$  sources with  $\text{Ly}\alpha$  fluxes  $\geq 4 \times 10^{-19} \text{ erg s}^{-1} \text{ cm}^{-2}$  in  $1 \text{ arcmin}^2$  between  $z \approx 2.8$  and  $\approx 6.7$ . In the redshift bin  $2.8 \leq z \leq 4$ , approximately 315 galaxies could be found in a DF survey, and only 15 are predicted to lie between  $z \approx 6$  and  $\approx 6.7$ . A DF survey would obtain the faintest LAE sample ever observed, pushing down the  $\text{Ly}\alpha$  luminosity function measurement towards the extreme faint end.

According to our mock catalogues, a MUSE MDF survey would lead to more than 2000 LAE detections within  $10 \text{ arcmin}^2$ . With about 10-h exposure per pointing, the  $\text{Ly}\alpha$  detection limit will reach  $\approx 10^{-18} \text{ erg s}^{-1} \text{ cm}^{-2}$  for the MDF, which is of the same order as

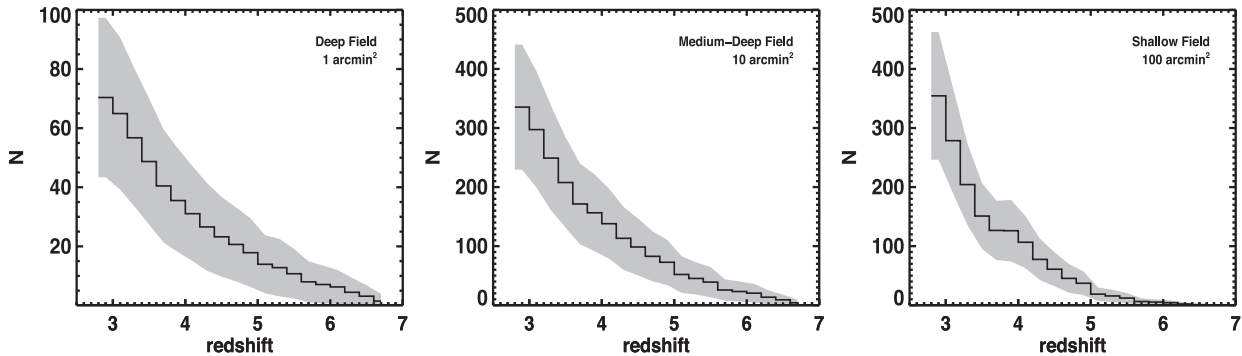


**Figure 5.** Predicted redshift distributions of  $\text{Ly}\alpha$ -emitting galaxies for typical MUSE DF (left:  $F_{\text{Ly}\alpha} \geq 4 \times 10^{-19} \text{ erg s}^{-1} \text{ cm}^{-2}$ ), MDF (centre:  $F_{\text{Ly}\alpha} \geq 10^{-18} \text{ erg s}^{-1} \text{ cm}^{-2}$ ), and SF (right:  $F_{\text{Ly}\alpha} \geq 10^{-17} \text{ erg s}^{-1} \text{ cm}^{-2}$ ) surveys between  $z = 2.8$  and  $6.7$ . The histograms show the mean number of objects in redshift bins of 0.2 dex, except the last one which is 0.1 dex wide, i.e.  $6.6 < z < 6.7$ . The grey shaded area illustrates the expected standard deviation computed from large numbers of lightcones.

**Table 1.** Mean number counts with standard deviation & median number counts with 10th/90th percentiles predicted for typical MUSE surveys: a DF ( $F_{\text{Ly}\alpha} \geq 4 \times 10^{-19} \text{ erg s}^{-1} \text{ cm}^{-2}$  –  $1 \text{ arcmin}^2$ ), a MDF ( $F_{\text{Ly}\alpha} \geq 10^{-18} \text{ erg s}^{-1} \text{ cm}^{-2}$  –  $10 \text{ arcmin}^2$ ), and an SF ( $F_{\text{Ly}\alpha} \geq 10^{-17} \text{ erg s}^{-1} \text{ cm}^{-2}$  –  $100 \text{ arcmin}^2$ ) survey.

	DF	MDF	SF	
Mean counts	$2.8 < z < 4$	$317 \pm 56$	$1417 \pm 208$	$1241 \pm 183$
	$4 < z < 5$	$119 \pm 31$	$505 \pm 110$	$327 \pm 69$
	$5 < z < 6$	$53 \pm 19$	$185 \pm 55$	$58 \pm 19$
	$6 < z < 6.7$	$15 \pm 9$	$47 \pm 23$	$7 \pm 5$
	$2.8 < z < 6.7$	$504 \pm 67$	$2155 \pm 241$	$1633 \pm 194$
Median counts	$2.8 < z < 4$	314 (248/389)	1411 (1158/1687)	1234 (1011/1477)
	$4 < z < 5$	117 (82/159)	497 (371/648)	325 (242/416)
	$5 < z < 6$	50 (30/78)	178 (120/260)	56 (35/83)
	$6 < z < 6.7$	14 (6/27)	42 (22/77)	6 (2/14)
	$2.8 < z < 6.7$	501 (418/590)	2146 (1852/2466)	1632 (1391/1883)

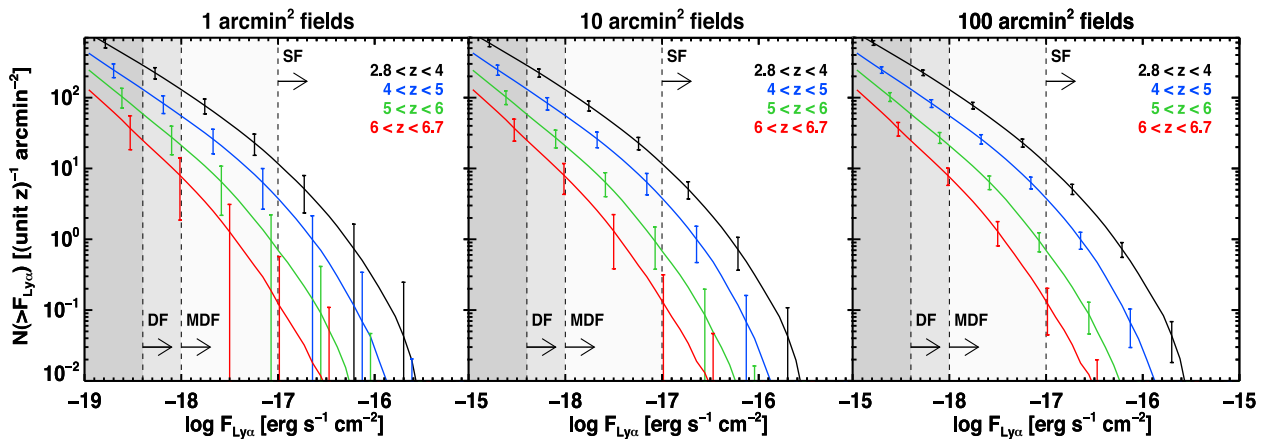


**Figure 6.** Mean number counts in mock fields of 1, 10, and 100 arcmin<sup>2</sup> (left-, centre, and right-hand panels, respectively). The curves show the predicted numbers of LAEs per unit redshift (see legend panel) and square arcminute in four redshift bins:  $2.8 < z < 4$ ,  $4 < z < 5$ ,  $5 < z < 6$ , and  $6 < z < 6.7$  (from top to bottom, as labelled). The error bars represent the standard deviation computed over a large number of lightcones. We add the limiting fluxes for typical Deep, Medium-Deep, and Shallow field surveys to be carried out with VLT/MUSE, labelled DF, MDF and SF, respectively.

previous surveys by Rauch et al. (2008), Cassata et al. (2011), and Dressler et al. (2015) whose samples contain 27, 217, and 210 LAEs, respectively. We predict that  $\approx 1500$  sources would be found in a MDF survey at  $2.8 < z < 4$ , and 500 at  $4 < z < 5$ , which would outnumber all existing spectroscopic surveys of faint LAEs. At  $5 < z < 6$ , we expect a bit less than 200 detections down to  $10^{-18}$  erg s<sup>-1</sup> cm<sup>-2</sup> in the MDF. In addition, we expect 45 LAEs at  $z \gtrsim 6$ . To sum up, we can expect a MDF survey to yield statistical samples in all the redshift ranges discussed here, allowing MUSE to put reliable constraints on the slope of the faint end of the Ly $\alpha$  LF, and its evolution, from  $z \approx 2.8$  to  $\approx 6.7$ .

Finally, more than 1500 LAEs would be detected between  $z \approx 2.8$  to  $\approx 6.7$  at fluxes larger than  $F_{\text{Ly}\alpha} \approx 10^{-17}$  erg s<sup>-1</sup> cm<sup>-2</sup> as part of a typical SF survey according to our model. This flux limit is typical of current Ly $\alpha$  NB surveys, and therefore, most constraints on the statistical properties of Ly $\alpha$ -emitting galaxies have been derived for such bright LAEs. For instance, the added samples of Ouchi et al. (2008) at  $z \approx 3.1 \pm 0.03$  and  $\approx 3.7 \pm 0.03$  contain nearly 460 LAE candidates, while approximately 1200 sources are expected at  $2.8 < z < 4$  in the SF survey from our mock catalogues (Table 1). At  $5 < z < 6$ , we predict 60 LAEs with  $F_{\text{Ly}\alpha} \gtrsim 10^{-17}$  erg s<sup>-1</sup> cm<sup>-2</sup> within 100 arcmin<sup>2</sup>. This is considerably less than in the NB survey of Ouchi et al. (2008) at  $z \approx 5.7 \pm 0.05$  ( $\approx 400$  objects), but comparable to the number of targeted sources in the follow-up observations of Kashikawa et al. (2011) and Hu et al. (2010), who built some of the largest spectroscopic samples to date at this redshift. Moreover, different NB surveys often use different filters set and selection criteria, while MUSE will build homogeneous samples of LAEs over a very large range of redshift. A SF survey would yield a unique, spectroscopic, large sample of bright LAEs allowing us to study the evolution of their statistical (e.g. abundances) and spectral properties from  $z \approx 2.8$  to  $\approx 6.7$ .

#### 4.2 Number count uncertainties

In addition to Table 1, we show our predicted number counts for typical DF, MDF, and SF MUSE surveys in four redshift bins in Fig. 6. For each field, we used mock lightcones of 1, 10, and 100 arcmin<sup>2</sup>, respectively, to compute the mean cumulative projected density of LAEs per unit redshift (curves) and the  $1\sigma$  standard deviation (error bars). We see that the standard deviation, computed

from thousands of lightcones, appears to be non-negligible, especially for the DF survey (left-hand panel), and at the bright-end of the MDF and SF surveys (middle and right-hand panels).

Here, the standard deviation is given by  $\sigma = \sqrt{\langle N^2 \rangle - \langle N \rangle^2}$ , where  $N$  is the number of sources in the mock lightcones in a given redshift range and above a given Ly $\alpha$  flux limit. Following Moster et al. (2011), we define the *relative cosmic variance*<sup>2</sup> as the uncertainty in excess to Poisson shot noise divided by the mean number of counts  $\langle N \rangle$ ,  $\sigma_{\text{v,rel}} = \sqrt{(\langle N^2 \rangle - \langle N \rangle^2 - \langle N \rangle) / \langle N \rangle}$ . Poisson noise normalized to  $\langle N \rangle$  can be expressed as  $\sigma_{\text{p,rel}} = \sqrt{\langle N \rangle} / \langle N \rangle$ . Using this simple formalism, we then attempt to quantify the respective contributions of Poisson noise and cosmic variance to number count uncertainties in the MUSE fields.

$\sigma_{\text{p,rel}}$  scales like  $1/\sqrt{\langle N \rangle}$ , hence it is large for small galaxy samples, and conversely, it tends to be 0 when the number of detections is large. The relative cosmic variance  $\sigma_{\text{v,rel}}$  reflects the uncertainty on the number counts due to field-to-field variation when probing a finite volume of the sky.

In Table 2, we show the predicted  $\sigma_{\text{p,rel}}$  and  $\sigma_{\text{v,rel}}$  in typical DF, MDF and SF surveys at different redshifts. We find that cosmic variance dominates the number count uncertainty in all cases. Its contribution is three to five times larger than the relative Poisson error at  $2.8 < z < 4$  in all fields. Both  $\sigma_{\text{p,rel}}$  and  $\sigma_{\text{v,rel}}$  values increase with increasing redshift, and at  $6 < z < 6.7$ , the difference is only a factor of 2–3 as Ly $\alpha$  sources are rarer at higher redshift in flux-limited surveys. On the one hand, although the DF survey is very deep, cosmic variance remains large due to the small volume that is probed. As an example, we show in Fig. 7 three mock realizations of a MUSE DF containing, respectively, 418 (upper panel: 10th percentile), 501 (middle panel: median number) and 590 (lower panel: 90th percentile) LAEs brighter than  $4 \times 10^{-19}$  erg s<sup>-1</sup> cm<sup>-2</sup>. On the other hand, a typical SF survey would cover a wider area (100 arcmin<sup>2</sup>), but its shallower depth only enables to observe rarer sources, enhancing (i) statistical uncertainties and (ii) cosmic variance as brighter LAEs are located in more massive, rarer,

<sup>2</sup> Here, we assume that the total variance,  $\sigma^2$  is the (quadratic) sum of cosmic variance and Poisson noise:  $\sigma_{\text{v}}^2 + \sigma_{\text{p}}^2$ . Relative cosmic variance is then written as  $\sigma_{\text{v,rel}} = \sigma_{\text{v}} / \langle N \rangle = \sqrt{\sigma^2 - \sigma_{\text{p}}^2} / \langle N \rangle = \sqrt{(\langle N^2 \rangle - \langle N \rangle^2 - \langle N \rangle) / \langle N \rangle}$  (see Moster et al. 2011, for more details).

**Table 2.** Predicted number count uncertainties for the DF, MDF, and SF surveys.  $\sigma_{p,rel}$  and  $\sigma_{v,rel}$  correspond to the relative Poisson error and the relative cosmic variance (Moster et al. 2011), respectively, (see the text for more details).

	DF		MDF		SF	
	$\sigma_{v,rel}$ (per cent)	$\sigma_{p,rel}$ (per cent)	$\sigma_{v,rel}$ (per cent)	$\sigma_{p,rel}$ (per cent)	$\sigma_{v,rel}$ (per cent)	$\sigma_{p,rel}$ (per cent)
$2.8 < z < 4$	16.7	5.6	14.4	2.7	14.5	2.8
$4 < z < 5$	24.4	9.1	21.3	4.4	20.4	5.5
$5 < z < 6$	33.1	13.7	28.8	7.4	30.0	13.1
$6 < z < 6.7$	54.1	25.8	46.7	14.6	60.6	37.8

haloes than fainter sources on average in our model (Garel et al. 2015). Accordingly, clustering analysis suggest that bright LAEs tend to be more clustered (Ouchi et al. 2003; Jose, Srianand & Subramanian 2013). We predict the relative uncertainties to be minimized for a typical MDF survey as it is a trade-off between volume size and flux depth. At  $2.8 < z < 4$ ,  $\sigma_{p,rel}$  and  $\sigma_{v,rel}$  are about 3 and 15 per cent, respectively, reaching  $\approx 15$  and 45 per cent in the  $z = 6-6.7$  redshift bin. Finally, we note that these values have to be seen as lower limits because of the finite volume of our simulation box.

These simple quantitative estimations suggest that uncertainties on the number counts will be non-negligible, and their accurate determination will be needed to derive robust constraints on the Ly $\alpha$  LFs.

### 4.3 Ly $\alpha$ luminosity and SFR densities

MUSE surveys will compile statistical, homogeneous samples of Ly $\alpha$ -emitting galaxies at several limiting fluxes over a large redshift range which will allow us to assess the contribution of faint sources to the global LAE population. In the next paragraphs, we therefore present our predictions for cosmic Ly $\alpha$  luminosity density and SFR as a function of redshift, that will be probed by typical MUSE surveys.

Fig. 8 shows the cosmic Ly $\alpha$  luminosity density  $\rho_{Ly\alpha}$  in four redshift bins,  $2.8 < z < 4$ ,  $4 < z < 5$ ,  $5 < z < 6$ , and  $6 < z < 6.7$ . First, we compare our predictions (red curve) to estimates from NB observations (shaded red area; Ouchi et al. 2008, 2010) for which the observed (uncorrected for dust) Ly $\alpha$  luminosity function is integrated down to  $L_{Ly\alpha} = 2.5 \times 10^{42}$  erg s $^{-1}$ . The model agrees well with the data at  $z = 3-5$  but seems a factor of 2 lower at higher redshift. As shown in the fig. 2 of Garel et al. (2015), our model reproduces reasonably well the observed Ly $\alpha$  luminosity functions from  $z = 3$  to 7, but it slightly underpredicts the abundances of LAEs reported by Ouchi et al. (2008, 2010) at  $z \approx 6$  (possibly due to high contamination in NB LAE samples at this redshift), hence the difference between the model and the data in Fig. 8.

Next, we present the redshift evolution of  $\rho_{Ly\alpha}$  as predicted by our model for the MUSE DF (solid black line), MDF, and SF surveys. Here, we computed  $\rho_{Ly\alpha}$  by summing up the contribution of galaxies in our mock catalogues above the limiting Ly $\alpha$  flux of each MUSE survey using lightcones of 10 arcmin $^2$ . First, we see that the SF survey (dotted light grey line) should be recovering a Ly $\alpha$  luminosity density roughly similar to what we predict for current NB surveys (red curve). This is not surprising because the SF Ly $\alpha$  sensitivity flux limit ( $F_{Ly\alpha} \geq 10^{-17}$  erg s $^{-1}$  cm $^{-2}$ ) corresponds to luminosities of  $\approx 8 \times 10^{41}$  erg s $^{-1}$  at  $z \approx 3$  and  $\approx 4 \times 10^{42}$  erg s $^{-1}$  at  $z \approx 6$ , which is of the same order as in typical NB surveys (Shimasaku et al. 2006; Ouchi et al. 2008; Shioya et al. 2009; Hu et al. 2010).

Secondly, we compare the predictions for the various MUSE surveys with one another. A typical MDF survey (dashed dark grey

line) would be able to detect Ly $\alpha$  line fluxes as low as  $10^{-18}$  erg s $^{-1}$  cm $^{-2}$ , that is 10 times fainter than in an SF survey. We clearly notice that the cosmic Ly $\alpha$  luminosity density probed by a MDF is expected to be much larger than for an SF survey and than what is currently available in NB surveys. For instance, between the SF and MDF surveys, we expect a gain in terms of  $\rho_{Ly\alpha}$  of a factor of  $\approx 2$  at  $z = 3$  and  $\approx 6$  at  $z = 6$ . With even longer exposure, a typical DF survey will reach Ly $\alpha$  fluxes down to  $4 \times 10^{-19}$  erg s $^{-1}$  cm $^{-2}$  and our model predicts an additional gain of 25–70 per cent at  $z = 3$  and 6 compared to the MDF.

Similar trends are seen in Fig. 9 where we plot the predicted cosmic SFR density,  $\rho_{SFR}$ , to be probed by typical MUSE surveys. Again, we see that deeper Ly $\alpha$  surveys are expected to unveil sources that make a significant contribution to the cosmic SFR density compared to existing samples of brighter LAEs. Compared to the SF survey, we predict that Ly $\alpha$ -emitting galaxies to be found in the MDF (DF) survey are likely to increase the global SFR budget by a factor of 2 at  $z \approx 3$  and a factor of 7 at  $z \approx 6$  ( $\times 2.5$  at  $z \approx 3$  and  $\times 10$  at  $z \approx 6$  for the DF survey).

Overall, we predict that the faint LAEs to be found in MUSE DF and MDF surveys make a larger contribution to the global cosmic Ly $\alpha$  luminosity density and SFR density compared to brighter galaxies seen in the SF survey or current wide-field NB surveys. The values quoted above remain somehow dependent on the exact faint-end slope of the Ly $\alpha$  luminosity function. The LF being still non-constrained at such extremely low fluxes, our predictions for the DF survey will need to be tested, in particular by MUSE surveys themselves. At  $z \approx 3$  and 6, the number counts predicted by our model reasonably agree with the data of Rauch et al. (2008) and Dressler et al. (2015, see Fig. 6), which reached Ly $\alpha$  fluxes of approximately  $10^{-18}$  erg s $^{-1}$  cm $^{-2}$ , so we expect our predictions for the MDF survey to be reliable enough.

In conclusion, it appears that a MUSE survey over 10 arcmin $^2$  down to  $F_{Ly\alpha} \geq 10^{-18}$  erg s $^{-1}$  cm $^{-2}$ , i.e. a MDF survey, represents an optimal strategy to probe a large fraction of SFR density and to minimize cosmic variance as it seems to provide the best trade-off between scientific gain and telescope time.

## 5 THE ROLE OF LAES IN THE HIERARCHICAL CONTEXT

In CDM cosmology, galaxy formation is described within the hierarchical clustering scenario in which DM haloes grow through the accretion of smaller structures. Hybrid models of galaxy formation, e.g. GALICS, are based on this scheme, and they use cosmological  $N$ -body simulations to follow the evolution of the DM density field. The identification of virialized haloes at each simulation output timestep, and the reconstruction of the history of these haloes are stored in order to compute the baryonic physics as a post-processing step, and then describe the evolution of galaxies. In this context, the

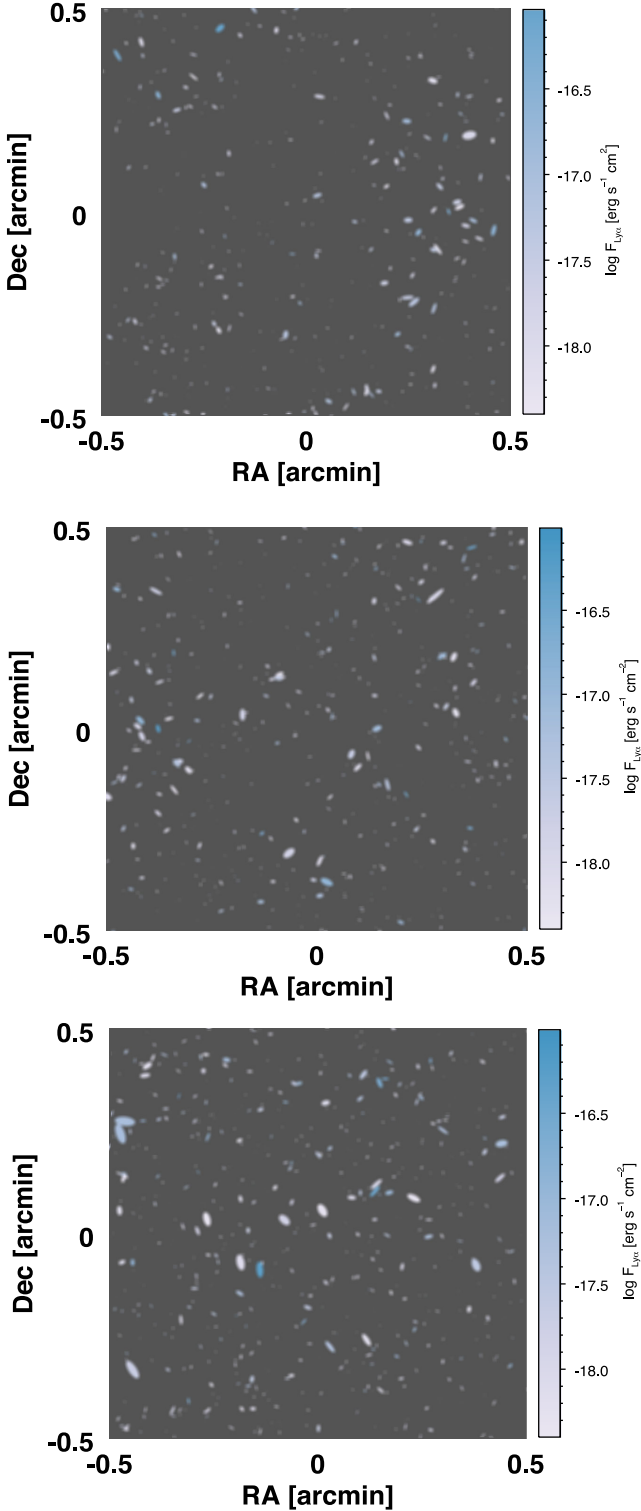


**Figure 7.** Mock maps for a typical MUSE DF of size  $1 \times 1 \text{ arcmin}^2$ . The three panels illustrate the variance in terms of number counts for different pointings. The middle panel shows a map where the number of galaxies is equal to the median value from 5000 mock fields of  $1 \text{ arcmin}^2$ . The upper and lower panels correspond to the 10th percentile and 90th percentile, respectively. Galaxies have been selected above a threshold of  $F_{\text{Ly}\alpha} \geq 4 \times 10^{-19} \text{ erg s}^{-1} \text{ cm}^{-2}$ , and lie in the redshift range  $2.8 < z < 6.7$ .

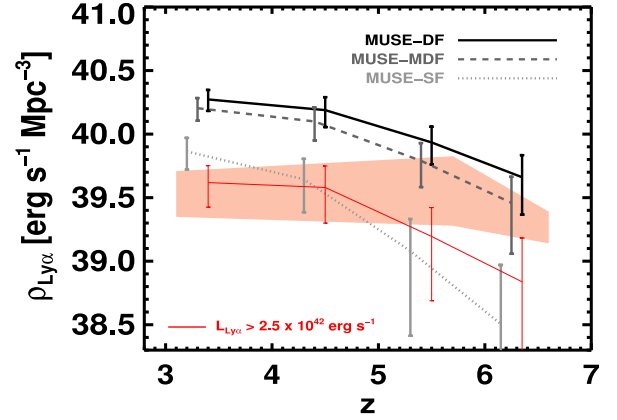


**Figure 8.** Evolution of the Ly $\alpha$  luminosity density. The black, dark grey, and light grey curves represent the Ly $\alpha$  luminosity density,  $\rho_{\text{Ly}\alpha}$ , that we expect to probe with typical MUSE Deep Field (DF- $F_{\text{Ly}\alpha} \geq 4 \times 10^{-19} \text{ erg s}^{-1} \text{ cm}^{-2}$ ), Medium-Deep Field (MDF- $F_{\text{Ly}\alpha} \geq 10^{-18} \text{ erg s}^{-1} \text{ cm}^{-2}$ ), and Shallow Field (SF- $F_{\text{Ly}\alpha} \geq 10^{-17} \text{ erg s}^{-1} \text{ cm}^{-2}$ ) surveys, respectively. Each curve shows the mean  $\rho_{\text{Ly}\alpha}$  measured from 5000 lightcones of  $10 \text{ arcmin}^2$  in four redshift bins:  $2.8 < z < 4$ ,  $4 < z < 5$ ,  $5 < z < 6$ , and  $6 < z < 6.7$ . The error bars correspond to the  $1\sigma$  standard deviations. The dark grey, and light grey curves have been shifted horizontally by 0.1 dex for the sake of clarity. The red curve shows the evolution of the Ly $\alpha$  luminosity density using a fixed Ly $\alpha$  luminosity threshold of  $L_{\text{Ly}\alpha} \geq 2.5 \times 10^{42} \text{ erg s}^{-1}$  which is typical of current NB wide-field surveys of LAEs, e.g. Ouchi et al. (2008, 2010, red shaded area).

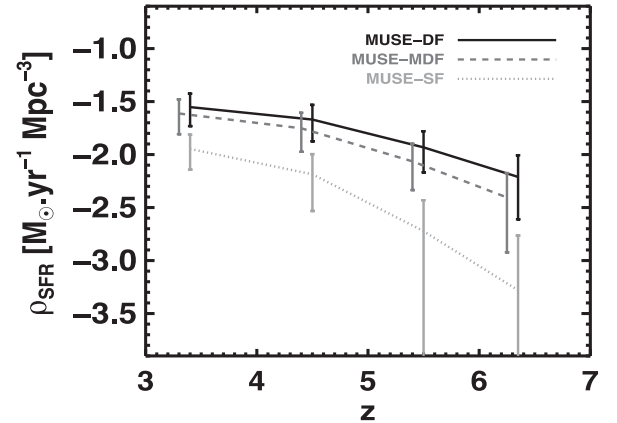


**Figure 9.** Evolution of the SFR density. The black, dark grey, and light grey curves represent the SFR density,  $\rho_{\text{SFR}}$ , that we expect to probe with the Ly $\alpha$ -emitting galaxies in typical MUSE Deep Field (DF- $F_{\text{Ly}\alpha} \geq 4 \times 10^{-19} \text{ erg s}^{-1} \text{ cm}^{-2}$ ), Medium-Deep Field (MDF- $F_{\text{Ly}\alpha} \geq 10^{-18} \text{ erg s}^{-1} \text{ cm}^{-2}$ ), and Shallow Field (SF- $F_{\text{Ly}\alpha} \geq 10^{-17} \text{ erg s}^{-1} \text{ cm}^{-2}$ ) surveys, respectively. Each curve shows the mean  $\rho_{\text{Ly}\alpha}$  measured from 5000 lightcones of  $10 \text{ arcmin}^2$  in four redshift bins:  $2.8 < z < 4$ ,  $4 < z < 5$ ,  $5 < z < 6$ , and  $6 < z < 6.7$ . The error bars correspond to the  $1\sigma$  standard deviations. The dark grey curve has been shifted horizontally by 0.1 dex for the sake of clarity.

hybrid method is thus an extremely powerful tool to study the formation and merging history of a population of galaxies.

In this section, we perform a merger tree analysis to investigate the connection between the host haloes of high-redshift LAEs and nowadays haloes. We identify in our simulation the  $z = 0$  descendants of high-redshift Ly $\alpha$  sources to be detected by the various MUSE surveys, and conversely, the progenitors of local objects, and in particular the building blocks of Milky Way (MW)-like haloes. In the following, we will focus on the progenitor/descendant link

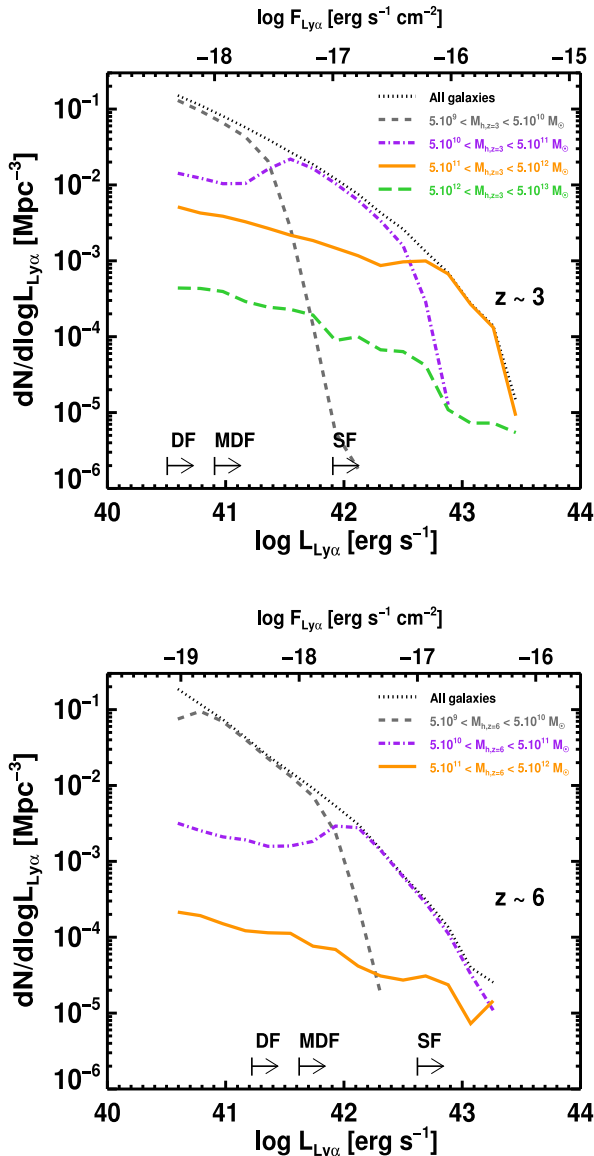


**Figure 10.**  $\text{Ly}\alpha$  luminosity function at  $z = 3$  (top panel) and  $z = 6$  (bottom panel). The dotted curve shows the total  $\text{Ly}\alpha$  LF, while the other curves distinguish between the mass of the host haloes of LAEs, as labelled.

between  $z = 0$  objects and the host haloes of LAEs at two epochs which somehow bracket the wavelength range where  $\text{Ly}\alpha$  will be detectable by MUSE,  $z = 3$  and 6.

### 5.1 The host haloes of LAEs at high redshift

Here, we explore the dynamical range spanned by LAEs at high redshift as a function of  $\text{Ly}\alpha$  luminosity as predicted by our model. In Fig. 10, we plot the  $\text{Ly}\alpha$  luminosity functions at  $z = 3$  and 6 and we highlight the contribution of subsamples of LAEs split by host halo mass. The first thing to note is that LAEs located in low-mass haloes make the faint-end of the  $\text{Ly}\alpha$  LF (short-dashed grey curve), while more massive haloes host brighter LAEs (dot-dashed purple, solid orange and long-dashed green curves). Hence, at a given redshift, deeper surveys probe lower mass haloes. This is simply because more massive haloes accrete more gas, so the galaxies they host have higher SFR, hence higher intrinsic  $\text{Ly}\alpha$

luminosity. In each range of halo mass, the highest  $\text{Ly}\alpha$  luminosity allowed is set by the maximal gas accretion rate taking place in most massive haloes. According to our model, LAEs currently seen by NB surveys ( $L_{\text{Ly}\alpha} \gtrsim 10^{42} \text{ erg s}^{-1}$ ) are predominantly hosted by haloes with masses of  $5 \times 10^{10-12} M_{\odot}$ . We expect the majority of faint sources in typical MUSE DF and MDF surveys to inhabit much less massive haloes, i.e.  $5 \times 10^9-10 M_{\odot}$ .

Secondly, for a given halo mass range, we see that the  $\text{Ly}\alpha$  LF extends to lower luminosities. In our model, we do not identify and neither follow substructures, so each halo may contain more than one galaxy. Massive haloes usually host one central galaxy and many satellites. As the gas supply from diffuse accretion only feeds the central galaxy of a given halo, satellites are more likely to display a fainter intrinsic emission than the central source. The extending tail towards low  $\text{Ly}\alpha$  luminosities is then mainly populated by the large number of satellites. Intrinsically  $\text{Ly}\alpha$ -bright, central, galaxies make an additional, though minor statistically speaking, contribution to this. As extensively discussed in Garel et al. (2015), the attenuation of the  $\text{Ly}\alpha$  line due to resonant scattering is small in low-mass LAEs because of their low dust content. However, the  $\text{Ly}\alpha$  escape fraction can be very low in more massive, intrinsically  $\text{Ly}\alpha$ -bright, objects with large H I column density and dust opacity, redistributing these galaxies at the faint end of the LF.

### 5.2 The descendants of the LAE host haloes

Using the information stored in the merger trees, we can now investigate the link between the host haloes of the high-redshift sources to be detected by typical MUSE surveys and their descendants in the local Universe. Fig. 11 shows the halo mass distributions of LAEs (thin red histograms) at  $z \approx 3$  (top panel) and  $z \approx 6$  (bottom panel) in the three surveys (DF, MDF, and SF). Unsurprisingly, the brightest  $\text{Ly}\alpha$  galaxies at high redshift, as those in the SF survey, are hosted by the most massive haloes (see Section 5.1). When fainter sources are considered (i.e. with the DF and MDF surveys), the host haloes sample the lower mass end of the halo mass function (HMF – thin red dashed lines). It is interesting to point out that the median mass of LAE haloes, illustrated by the vertical dotted lines, evolves weakly from  $z \approx 6$  to  $\approx 3$  for all three samples considered here. At both redshifts, the (log) median halo mass is approximately 10.3, 10.7 and 11.3  $M_{\odot}$  in the DF, MDF, and SF surveys, respectively.<sup>3</sup>

In each panel of Fig. 11, we also plot the descendant halo distributions at  $z = 0$  (thick blue histograms) for each corresponding LAE sample. Again, we see that the descendants of the haloes of the brightest high-redshift LAEs make the high-mass end of the  $z = 0$  HMF (thick blue dashed line), whereas the hosts of fainter  $\text{Ly}\alpha$  sources evolve into less massive haloes on average. The descendants of LAEs in the DF and MDF surveys at  $z \approx 3$  span a mass range from  $\approx 10^{10}$  to  $10^{15} M_{\odot}$ , with a median value around  $10^{11} M_{\odot}$ . The brighter sources of the SF survey are predicted to end up in haloes more massive than  $10^{11} M_{\odot}$  at  $z = 0$ , with a median mass of  $\approx 2 \times 10^{12} M_{\odot}$  which corresponds to the upper limit estimate of the MW halo mass (grey stripe) reported by Battaglia et al. (2005).

At  $z \approx 6$ , we predict that a typical SF survey would probe haloes that have very massive descendants at  $z = 0$  ( $M_{\text{h}}^{\text{med}} \approx 5 \times 10^{13} M_{\odot}$ ), e.g. group/cluster galaxy haloes. The DF and MDF

<sup>3</sup> For the halo mass distributions shown in Fig. 11, we only count haloes (resp. halo descendants) which contain at least one galaxy (resp. one progenitor galaxy) brighter than  $F_{\text{Ly}\alpha}^{\text{limit}}$ . Given that massive haloes are more likely to host more than one galaxy, the median halo masses that we quote would be higher if we were associating one halo to each LAE instead.

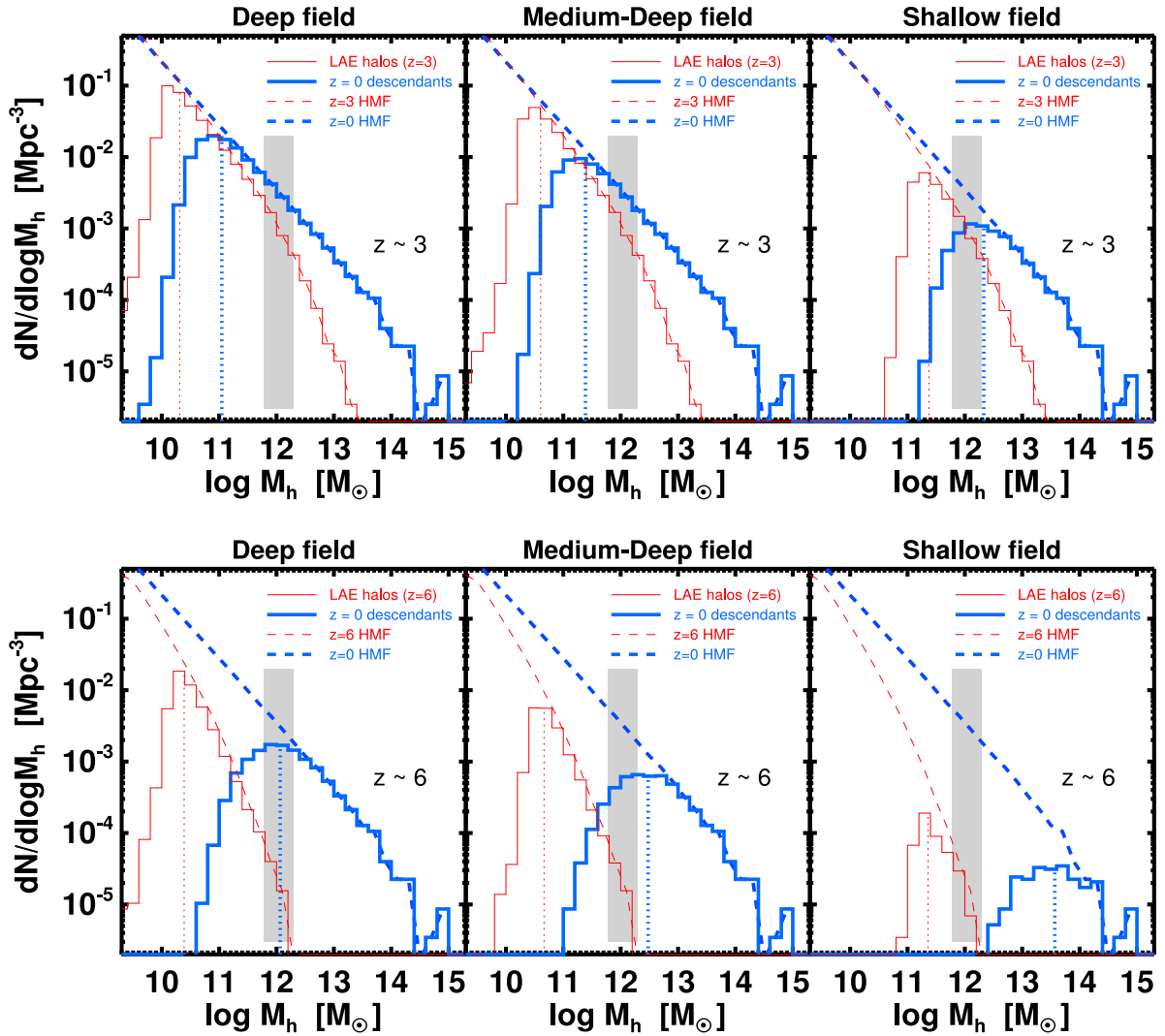


**Figure 11.** Halo mass distributions of the  $z = 0$  descendants of LAEs at  $z \approx 3$  (top panels) and  $\approx 6$  (bottom panels). The left-hand, middle, and right-hand panels correspond to LAEs selected in typical DF ( $F_{\text{Ly}\alpha} \geq 4 \times 10^{-19} \text{ erg s}^{-1} \text{ cm}^{-2}$ ), MDF (middle:  $F_{\text{Ly}\alpha} \geq 10^{-18} \text{ erg s}^{-1} \text{ cm}^{-2}$ ), and SF (bottom:  $F_{\text{Ly}\alpha} \geq 10^{-17} \text{ erg s}^{-1} \text{ cm}^{-2}$ ) surveys. The thin red histograms represent the distribution of the LAE host haloes, while the thick blue histograms show their descendants at  $z = 0$ . The median masses of each distribution are represented by a vertical dotted line. The thin red and thick blue dashed lines illustrate the total HMF at  $z = 3/6$  and  $0$ , respectively. The mass estimate of the MW halo is shown by the grey shaded area ( $6 \times 10^{11} < M_{h,z=0} < 2 \times 10^{12} M_{\odot}$ ; Battaglia et al. 2005).

surveys are expected to probe LAEs which evolve into lower mass haloes at  $z = 0$  ( $\gtrsim 10^{11} M_{\odot}$ ), with median masses of the same order as the MW DM halo (i.e.  $M_h \approx 10^{12} M_{\odot}$ ; Battaglia et al. 2005; McMillan 2011; Phelps, Nusser & Desjacques 2013; Kafle et al. 2014).

### 5.3 The high-redshift progenitors of $z = 0$ haloes

Having discussed the local descendants of LAE host haloes at different Ly $\alpha$  luminosities in the previous section, we now attempt to assess how LAEs trace the progenitors of  $z = 0$  haloes. This is illustrated in Fig. 12 where we show the Ly $\alpha$  LFs at  $z = 3$  (top panel) and  $z = 6$  (bottom panel) for three halo mass ranges at  $z = 0$ . In both panels, the dotted black curves give the total Ly $\alpha$  LF, whereas the dot-dashed purple, solid orange, and long-dashed green curves correspond to the distribution of the progenitors of haloes with masses of  $5 \times 10^9 < M_{h,z=0} < 5 \times 10^{11}$ ,  $5 \times 10^{11} < M_{h,z=0} < 5 \times 10^{13}$ , and  $5 \times 10^{13} < M_{h,z=0} < 5 \times 10^{15} M_{\odot}$ .

According to our model, the progenitors of haloes in the lowest mass bin are mainly hosting faint LAEs at high redshift (i.e.  $L_{\text{Ly}\alpha} \lesssim 10^{42} \text{ erg s}^{-1}$ ). These objects are nearly never detected in typical NB surveys at  $z = 3\text{--}6$  or in the HETDEX spectroscopic pilot survey ( $z \lesssim 3.8$ ; Blanc et al. 2011), and are unlikely to be probed in a MUSE SF survey. Typical DF and MDF surveys would probe these faint LAEs, adding up to the existing samples of Rauch et al. (2008), Cassata et al. (2011), and Dressler et al. (2015).

The most massive haloes at  $z = 0$  (green curves), corresponding mainly to the hosts of massive early-type galaxies (van den Bosch, Yang & Mo 2003; Mandelbaum et al. 2006; Yang, Mo & van den Bosch 2009), are predicted to be made up of the brightest LAEs at high redshift. The bulk of their progenitors is however composed of fainter Ly $\alpha$  sources, that are either (i) satellite galaxies in massive haloes at high redshift, or (ii) central galaxies in low-mass haloes which were accreted to form very massive haloes towards  $z = 0$  through hierarchical merging. The Ly $\alpha$  distribution of the progenitors of the medium-mass haloes (orange curves) spans a similar range, from the highest luminosities towards the faint end,

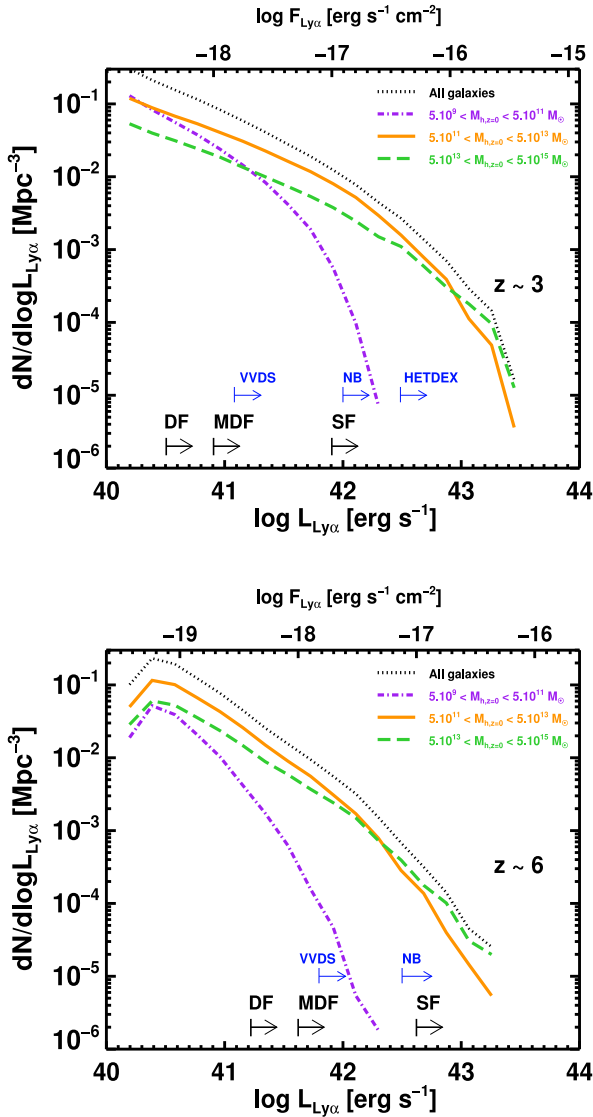


**Figure 12.**  $\text{Ly}\alpha$  luminosity function at  $z = 3$  (top panel) and  $z = 6$  (bottom panel). The dotted curve shows the total  $\text{Ly}\alpha$  LF. The other curves correspond to the  $\text{Ly}\alpha$  luminosity distributions of LAEs residing in the progenitors of  $z = 0$  haloes divided in three mass ranges (see legend). Black arrows with labels illustrate the  $\text{Ly}\alpha$  detection limits of typical MUSE DF, MDF, and SF surveys. For comparison, we include the minimum  $\text{Ly}\alpha$  fluxes (blue arrows) reached by the VVDS (Cassata et al. 2011), by the HETDEX pilot survey (Blanc et al. 2011), and by current NB surveys (using the thresholds of Ouchi et al. 2008, at  $z = 3.1$  and 5.7).

but is steeper than for very massive haloes. These intermediate-mass haloes are thought to be predominantly the locus of  $L^*$ , late-type galaxies like our Galaxy, as the range  $5 \times 10^{11} < M_{h,z=0} < 5 \times 10^{13} M_{\odot}$  broadly encompasses the halo mass of an MW-like galaxy, estimated to be  $0.8^{+1.2}_{-0.2} \times 10^{12} M_{\odot}$  (Battaglia et al. 2005). Nevertheless, we see from Fig. 12 that the distributions of LAEs residing in the progenitors of  $z = 0$  objects vary quickly as a function of halo mass, so the orange curve might not represent accurately the predicted progenitors distribution of MW-like objects. We will then concentrate on the progenitors of MW-like haloes in the next section, and we will compare our results with other theoretical studies (e.g. Gawiser et al. 2007; Salvadori, Dayal & Ferrara 2010) in Section 6.

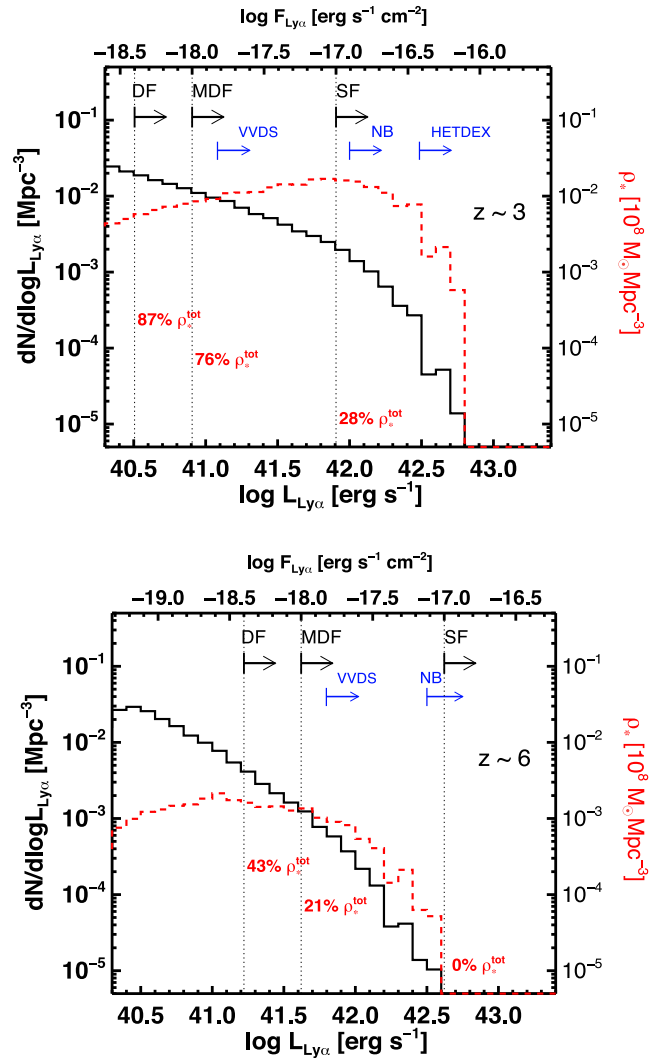


**Figure 13.** Distribution of the LAEs residing in the progenitor haloes of MW-like haloes at  $z \approx 3$  (top panel) and  $z \approx 6$  (bottom panel). In each panel, the black histogram shows the  $\text{Ly}\alpha$  luminosity distribution of the galaxies hosted by the progenitors of MW-like haloes, while the red histogram gives the SMD per  $L_{\text{Ly}\alpha}$  bin. The arrows show the  $\text{Ly}\alpha$  flux limits of the three typical MUSE fields (black) and others existing surveys (see caption of Fig. 12). The red labels represent the fraction of the total SMD sitting in the progenitors of MW-like haloes,  $\rho_*^{\text{tot}}$ , that can be probed by LAEs in the different typical MUSE surveys.

#### 5.4 The high-redshift progenitors of MW-like haloes

In Fig. 13, we plot the  $\text{Ly}\alpha$  luminosity distribution (black histogram) at  $z \approx 3$  and  $z \approx 6$  of the LAEs residing in the progenitors of  $z = 0$  haloes with  $6 \times 10^{11} < M_{h,z=0} < 2 \times 10^{12} M_{\odot}$ , that we define as MW-like haloes in what follows. We first note that current NB surveys are only able to probe the progenitors of MW-like haloes which host LAEs with  $\text{Ly}\alpha$  luminosities  $\gtrsim 10^{42} \text{ erg s}^{-1}$  at  $z \approx 3$  and  $z \approx 6$ . The vast majority of the progenitors of MW-like haloes contain LAEs with fainter luminosities, which number density keeps increasing towards lower values, even below the MUSE DF limit. In the bottom panel of Fig. 13 ( $z \approx 6$ ), the apparent flattening of the distribution at  $L_{\text{Ly}\alpha} \approx 3 \times 10^{40} \text{ erg s}^{-1}$  is due to the limit of resolution of our simulation, and the curve would start decreasing at

lower luminosities (see Section 2.5). At  $z \approx 3$  (top panel), a similar effect would be seen at  $L_{\text{Ly}\alpha} \lesssim 2 \times 10^{40} \text{ erg s}^{-1}$ . In practice, this means that we *miss* galaxies located in haloes less massive than our resolution limit, and the number distribution of LAEs should keep increasing down to lower luminosities if we were using a higher resolution simulation. Even though these very faint LAEs are obviously more numerous than the sources to be detected by MUSE surveys, they consist of low-mass objects, forming stars at a very low rate, and they represent a small fraction of the overall SFR and stellar mass budget.

To illustrate this point, we also show on Fig. 13 the stellar mass density (SMD) in the high-redshift progenitors of MW-like haloes per bin of  $\log L_{\text{Ly}\alpha}$ ,  $\rho_*$  (red histogram). Given that stellar mass is well correlated to SFR (see Fig. 2), and that the intrinsic Ly $\alpha$  intensity is directly proportional to SFR to first order (see e.g. equation 8 of Barnes, Garel & Kacprzak 2014), it is not surprising that the brightest LAEs make a significant contribution to the SMD. As shown on Fig. 13,  $\rho_*$  increases faster than the number density from high-to-low Ly $\alpha$  luminosities. This is especially true at  $z \approx 3$ , where  $\rho_*$  reaches a maximum at  $L_{\text{Ly}\alpha} \approx 10^{42} \text{ erg s}^{-1}$ , and starts declining towards fainter Ly $\alpha$  luminosities. This roughly corresponds to the SF survey limit ( $F_{\text{Ly}\alpha} \geq 10^{-17} \text{ erg s}^{-1} \text{ cm}^{-2}$ ), and the model predicts that 28 per cent of the total SMD sitting in the progenitors of MW-like haloes can be probed in this case. A significantly higher fraction is expected to be recovered from faint LAEs in typical MDF and DF surveys (i.e.  $0.76\rho_*^{\text{tot}}$  and  $0.87\rho_*^{\text{tot}}$ , respectively). This implies that these deep surveys could probe the bulk of the  $z = 3$  progenitors of local galaxies like ours according to our model. At  $z \approx 6$ , the progenitors of the MW-like haloes will not be traced by LAEs in an SF survey. However, we expect the LAE sample of an MDF survey to contain about 21 per cent of the total SMD in the progenitors of MW-like haloes. Moreover, almost half of the stars present in the  $z = 6$  progenitors of MW-like haloes should be sitting in LAEs detectable in a typical DF survey.

As mentioned earlier, the resolution limit of our simulation implies that our sample of LAEs is not complete below a given Ly $\alpha$  flux, as we miss galaxies which should form in haloes less massive than  $M_{\text{halo}}^{\text{min}}$ . The real value of  $\rho_*^{\text{tot}}$  is then unknown, so the absolute contributions to the SMD quoted in the previous paragraph must be viewed as upper limits. Determining  $\rho_*^{\text{tot}}$  accurately is quite uncertain since we would need to make assumptions about the number density of extremely faint galaxies and the halo mass at which galaxy formation is prevented (e.g. due to photoheating from the ionizing background; Okamoto et al. 2008).

Nevertheless, if we look at the relative contribution to the SMD between the different typical MUSE surveys, we are no longer affected by mass resolution effects. We then compare the SMD probed by typical MUSE surveys relatively to the NB surveys of Ouchi et al. (2008) at  $z \approx 3$  ( $F_{\text{Ly}\alpha} \geq 1.2 \times 10^{-17} \text{ erg s}^{-1} \text{ cm}^{-2}$ ) and  $z \approx 6$  ( $F_{\text{Ly}\alpha} \geq 8 \times 10^{-18} \text{ erg s}^{-1} \text{ cm}^{-2}$ ). At  $z \approx 3$ , the SF, MDF, and DF surveys are predicted to recover a stellar mass content in LAEs hosted by the progenitors of MW-like haloes  $\approx 1.25$ , 3, and 4 times larger than the NB survey of Ouchi et al. (2008). At  $z \approx 6$ , we find that Ouchi et al. (2008) only probe the very-bright end of the Ly $\alpha$  LF so these numbers go up to 100 and 200 for the MDF and DF surveys, respectively. Comparing instead with the VVDS survey which obtained the faintest existing sample at this redshift, we expect the fraction of the total mass density in LAEs located in the progenitors of MW-like haloes to be  $\approx 1.5$  and 3.5 times larger for typical MDF and DF surveys, respectively.

## 6 DISCUSSION

The role of high-redshift LAEs in the mass assembly of local galaxies has been discussed in a few previous studies, based either on the redshift evolution of the observed LAE bias, cosmological simulations, or a combination of them. Gawiser et al. (2007) performed a clustering analysis on 162  $z = 3.1$  LAEs from the sample of Gronwall et al. (2007), and they derived a median halo mass  $M_{\text{h}}^{\text{med}} \approx 10^{11} M_{\odot}$ . For comparison, Kovač et al. (2007) find  $M_{\text{h}}^{\text{med}} \approx 1.5\text{--}3 \times 10^{11} M_{\odot}$  at  $z = 4.5$ , and Ouchi et al. (2010) report that the host DM haloes of LAEs remain in the range  $10^{11 \pm 1} M_{\odot}$  from  $z \approx 3\text{--}7$ . For similar LAE selection ( $L_{\text{Ly}\alpha} \gtrsim$  a few  $10^{42} \text{ erg s}^{-1}$  and  $\text{EW}_{\text{Ly}\alpha} \gtrsim 20 \text{ \AA}$ ), we find that  $M_{\text{h}}^{\text{med}}$  increases from 1 to  $3 \times 10^{11} M_{\odot}$  from  $z \approx 6$  to  $\approx 3$ , in broad agreement with the observations (see section 6 of Garel et al. 2015, for more details). A more robust way to assess the expected  $L_{\text{Ly}\alpha}$ – $M_{\text{h}}$  relation is to quantitatively examine the spatial distribution of LAEs and compare with observational data. To this aim, we will investigate the two-point correlation functions of LAEs in a future study (Garel et al., in preparation).

Using merger trees from the MilliMillennium simulation, Gawiser et al. (2007) identify the  $z = 0$  descendants of LAEs at  $z \approx 3$  to have a median halo mass of  $\approx 1.2 \times 10^{12} M_{\odot}$ . This reasonably matches our predictions for a MUSE SF survey ( $M_{\text{h}}^{\text{med}} \approx 2 \times 10^{12} M_{\odot}$ ; top-right panel of Fig. 11), which is expected to detect similar LAEs as the ones investigated by Gawiser et al. (2007). Part of the difference might be due to the different cosmology assumed in the studies (based on WMAP-1 and WMAP-5 releases, respectively). In addition, Gawiser et al. (2007) used the minimum LAE host halo mass derived from their clustering analysis,  $3 \times 10^{11} M_{\odot}$ , to perform the merger tree study, whereas we use the full information provided by our model, i.e. the Ly $\alpha$  luminosities of galaxies and their DM host haloes. Using the same data as Gawiser et al. (2007), Walker-Soler et al. (2012) developed abundance-matching models of LAEs to track their evolution in the Millennium-II simulation. They also report that descendants of  $z \approx 3$  LAEs selected above  $L_{\text{Ly}\alpha} \gtrsim 10^{42} \text{ erg s}^{-1}$  have halo masses typical of L\*-galaxies, i.e.  $\approx 10^{12} M_{\odot}$ .

A complementary question is to wonder if high-redshift LAEs are located in the main progenitors of present-day MW-like haloes. In Section 5.4, we tracked the progenitors of MW-like haloes at  $z = 3$  and 6 using our merger trees, and we found that the brightest sources in these haloes have  $L_{\text{Ly}\alpha} \approx 5 \times 10^{42} \text{ erg s}^{-1}$ , while most progenitors of MW-like haloes host faint LAEs. Similar results are reported by Yajima et al. (2012b) who combined a cosmological hydrodynamical simulation with 3D RT calculations of the 60 most massive progenitors at  $z \lesssim 10$  (see their fig. 7). The study of Yajima et al. (2012b) focused on one single MW-like galaxy (and their progenitors) in a zoomed-in region and their initial conditions were set especially to model an MW-sized galaxy at  $z = 0$ . Contrary to them, we have identified all MW-like host haloes according to their mass in our simulation and looked at their high- $z$  building blocks, which allows us to investigate their properties in a statistical way. We discussed in Section 5.4 their predicted Ly $\alpha$  luminosity distribution and stellar mass density. From our model, we can also try to estimate, for a given LAE survey, what fraction of MW-like haloes will have high-redshift progenitors that are detectable through the LAEs they contain. From Table 3, the fraction of MW-like haloes *with at least one LAE host halo as progenitor* at  $z \approx 3$  in the DF, MDF surveys is very high, i.e. 0.97 and 0.96, respectively. This fraction is  $\approx 4$  times larger than for the SF or typical NB surveys. At  $z \approx 6$ ,

**Table 3.** Column (1) gives the fraction of MW-like  $z = 0$  haloes with one or more progenitor haloes at  $z = 3$  and 6, irrespectively from the  $\text{Ly}\alpha$  flux of the galaxy they host (i.e.  $F_{\text{Ly}\alpha} \geq 0 \text{ erg s}^{-1} \text{ cm}^{-2}$ ). Columns (2), (3) and (4) correspond to LAEs detectable in typical DF, MDF, and SF surveys. Column (5) corresponds to LAEs detectable with an observed  $\text{Ly}\alpha$  luminosity greater than  $10^{42} \text{ erg s}^{-1}$ . The first two rows show the fractions of MW-like haloes which progenitors have an LAE selected above the quoted  $\text{Ly}\alpha$  flux/luminosity limits only. The two last rows show the fractions for LAEs which are also detectable as LBG in typical dropout surveys (i.e. with an absolute rest-frame UV magnitude at  $1500 \text{ \AA}$  brighter than  $-18$ ; Bouwens et al. 2007; van der Burg, Hildebrandt & Erben 2010; Duncan et al. 2014).

		Fraction of MW-like haloes with at least one progenitor at $z \approx 3$ and $\approx 6$ .				
		$F_{\text{Ly}\alpha} \geq 0^{(1)}$	DF <sup>(2)</sup>	MDF <sup>(3)</sup>	SF <sup>(4)</sup>	$L_{\text{Ly}\alpha} \geq 10^{42} \text{ (5)}$
Ly $\alpha$ flux/lum. cut only	$z \approx 3$	0.98	0.97	0.96	0.30	0.20
	$z \approx 6$	0.97	0.50	0.16	0.00	0.025
Ly $\alpha$ flux/lum. cut & $M_{1500} < -18$	$z \approx 3$	0.44	0.43	0.43	0.30	0.19
	$z \approx 6$	0.09	0.09	0.08	0.00	0.025

we predict that about half of present-day MW-like haloes will have a progenitor hosting an LAE in the DF survey.

For an  $\text{Ly}\alpha$  detection threshold of  $L_{\text{Ly}\alpha} \gtrsim 10^{42} \text{ erg s}^{-1}$ , Salvadori et al. (2010) found that up to 68 per cent of MW-like haloes have at least one LAE host halo as a progenitor at  $z \approx 6$ , while we find the percentage to be less than 3 per cent. The origin of the discrepancy is not obvious but it might come from the different definition of the  $z = 0$  MW-like object used in this paper and in the study of Salvadori et al. (2010). Here, we used a hybrid model of galaxy formation that can match the  $\text{Ly}\alpha$  luminosity functions from  $z \approx 3$  to 7 and we searched for galaxies located in haloes at high redshift that are the progenitors of local haloes, only selected from their mass ( $6 \times 10^{11} < M_{\text{h}, z=0} < 2 \times 10^{12} M_{\odot}$ ). The model of Salvadori et al. (2010), based on the extended Press–Schechter theory, was instead adjusted to reproduce the  $z = 0$  properties our Galaxy (e.g. stellar mass and metallicity) and its local environment, which corresponds to a high-density region. As they are investigating a highly biased region of the Universe, their predicted LAE abundance at  $z \approx 6$  is much larger than the *mean* number density as observed in current NB  $\text{Ly}\alpha$  surveys.

In spite of the differences between the results of Salvadori et al. (2010) and ours, which suggest that the contours of the population of MW-like progenitors might highly depend on how we define an MW-like galaxy and its environment, it is interesting to note that both models predict that almost all progenitors of MW-like haloes traced by LAEs with  $L_{\text{Ly}\alpha} \gtrsim 10^{42} \text{ erg s}^{-1}$  should also be probed in typical LBG surveys with  $M_{1500} \lesssim -18$ . We find that this is also true for all LAEs in the SF (see Table 3). This seems very consistent with the work of González et al. (2012), based on the Durham model, who finds that an MW-like galaxy has a 95 per cent (70 per cent) probability of having at least one LBG with  $M_{1500} \lesssim -18.8$  as a progenitor at  $z \approx 3.5$  ( $z \approx 6.5$ ). According to our model, only a smaller fraction of the  $\text{Ly}\alpha$  sources expected in deeper surveys, such as the DF and MDF, should have  $M_{1500} \lesssim -18$ , although they should be detectable in very deep UV-selected surveys (e.g. Bouwens et al. 2015).

As discussed in Section 2.4, a noticeable outcome of our  $\text{Ly}\alpha$  RT modelling in expanding shells is that the IGM becomes transparent to  $\text{Ly}\alpha$  photons emerging from galaxies. Assuming alternative scenarios in which most of the  $\text{Ly}\alpha$  flux emerges from galaxies close to the line centre (e.g. a Gaussian profile centred on  $\lambda_{\text{Ly}\alpha}$ , or even a blue-shifted line in the presence of gas infall for instance), it would no longer be the case, especially at  $z \gtrsim 6$  when reionization is not necessarily complete yet. The impact on the visibility of LAEs would then depend on many factors, such as the exact form of the intrinsic  $\text{Ly}\alpha$  line, feedback, SFR, source clustering, or the

structure, the kinematics, and the ionization state of the local IGM (e.g. Dijkstra et al. 2007; McQuinn et al. 2007; Iliev et al. 2008; Dayal & Libeskind 2012; Hutter, Dayal & Müller 2015). As for the present study, should the  $\text{Ly}\alpha$  transmission be much less than unity, LAEs may appear fainter and less progenitors of MW-like haloes would be detectable with MUSE compared to the values quoted in Section 5.4. Similarly, MUSE surveys would thus probe a lower fraction of the global stellar mass budget located in the progenitors of MW-like haloes.

Disentangling internal  $\text{Ly}\alpha$  RT effects and IGM transmission remains a complicated issue, which cannot be easily constrained directly by observations. Nevertheless, theoretical studies have shown that outflows can dramatically alter the shape and the position of the peak of the  $\text{Ly}\alpha$  line (e.g. Santos 2004; Verhamme et al. 2006; Dijkstra, Mesinger & Wyithe 2011). Observationally, asymmetric profiles as well as velocity offsets between  $\text{Ly}\alpha$  and the systemic redshift are commonly measured both at high and low redshift (e.g. Kunth et al. 1998; Shapley et al. 2003; McLinden et al. 2011; Wofford, Leitherer & Salzer 2013; Rivera-Thorsen et al. 2015), which suggests that the IGM is not necessarily the cause of the flux reduction (or suppression) of the blue side of the  $\text{Ly}\alpha$  line and the velocity shift of the peak.

## 7 SUMMARY AND CONCLUSIONS

In this paper, we presented model predictions for high-redshift  $\text{Ly}\alpha$  galaxies to be observed through a typical wedding cake observing strategy with MUSE from  $z \approx 2.8$  to  $\approx 6.7$ . We used the GALICS hybrid model to describe the formation and evolution of galaxies in the cosmological context and a grid of numerical models to compute the RT of  $\text{Ly}\alpha$  photons through dusty gas outflows. This model can reasonably reproduce the abundances of  $\text{Ly}\alpha$  emitters and LBG (Garel et al. 2015), as well as the SMF (Section 2.3), in the redshift range where MUSE will be able to probe the  $\text{Ly}\alpha$  emission line. We built mock lightcones of LAEs corresponding to typical DF, MDF, and SF surveys over 1, 10, 100 arcmin<sup>2</sup>, and down to  $\text{Ly}\alpha$  fluxes of  $4 \times 10^{-19}$ ,  $10^{-18}$ , and  $10^{-17} \text{ erg s}^{-1} \text{ cm}^{-2}$ , respectively.

A DF survey would yield the faintest statistical sample of LAEs ever observed, allowing us to investigate the extreme faint slope of the  $\text{Ly}\alpha$  LF at high redshift. From our mock catalogues, we predict that  $\approx 500$  sources can be found between  $z \approx 2.8$  and  $z \approx 6.7$ . At  $F_{\text{Ly}\alpha} \gtrsim 10^{-18} \text{ erg s}^{-1} \text{ cm}^{-2}$ , our model agrees well with the abundances of faint LAEs reported by Rauch et al. (2008) and Dressler et al. (2015) which suggest a steep faint-end slope of the  $\text{Ly}\alpha$  LF. MUSE is expected to compile a large sample of such faint sources, as we predict  $\approx 2000$  LAEs to be detected in a typical

MDF survey. Furthermore, 1500 LAEs should be discovered in 100 arcmin<sup>2</sup> with a shallower survey at fluxes greater than  $\approx 10^{-17}$  erg s<sup>-1</sup> cm<sup>-2</sup>. Overall, we find that the main source of uncertainty will be cosmic variance, as it is often the case in small-volume, pencil-beam, surveys. In addition, our results suggest that the very faint galaxies to be seen in MUSE surveys, and usually missed by current optical surveys, will contribute significantly to the cosmic SFR budget at  $z \approx 3-7$ .

Based on our  $N$ -body DM simulation, we performed a merger tree analysis to assess the role of LAEs, and especially faint ones, in the hierarchical scenario of structure formation. We thus explored the link between the host haloes of MUSE LAEs at high redshift and haloes in the local Universe. On the one hand, we predict that bright LAEs ( $F_{\text{Ly}\alpha} \gtrsim 10^{-17}$  erg s<sup>-1</sup> cm<sup>-2</sup>) evolve, on average, into massive haloes at  $z = 0$ , typical of host haloes of massive ellipticals or galaxy groups. On the other hand, we find that faint LAEs at  $z \approx 3$  ( $z \approx 6$ ) from typical DF and MDF surveys have a median halo mass of  $\approx 10^{11} M_{\odot}$  ( $\approx 10^{12} M_{\odot}$ ), comparable to the haloes of sub- $L^*$  ( $L^*$ ) galaxies at  $z = 0$ . Finally, our study predicts that a large fraction of the high-redshift progenitors of MW-like haloes can be probed by these surveys. For instance, a survey at  $F_{\text{Ly}\alpha} \gtrsim 4 \times 10^{-19}$  erg s<sup>-1</sup> cm<sup>-2</sup> is expected to probe the bulk of the global stellar mass budget enclosed in the  $z \approx 3$  progenitors of MW-like host haloes.

In this paper, we have shown that deep surveys, e.g. with MUSE, can efficiently probe the population of faint Ly $\alpha$ -emitting galaxies at high redshift. The understanding of the formation and evolution of these sources appears to be essential to get insight into the mass assembly of local objects, such as the MW. In a future study, we will keep investigating the physical and spectral properties of galaxies in the early Universe fed by forthcoming MUSE data, as well as optical *HST* surveys (e.g. Bouwens et al. 2015) and spectroscopic redshift surveys (e.g. Le Fèvre et al. 2015).

Mock catalogues and LAE number count predictions from Figs 4 and 6 are available at <http://cral.univ-lyon1.fr/labo/perso/thibault.garel/>.

Additional information is available upon request at: [thibault.garel@univ-lyon1.fr](mailto:thibault.garel@univ-lyon1.fr).

## ACKNOWLEDGEMENTS

We thank the anonymous referee for his/her comments. TG is grateful to the LABEX Lyon Institute of Origins (ANR-10-LABX-0066) of the Université de Lyon for its financial support within the programme ‘Investissements d’Avenir’ (ANR-11-IDEX-0007) of the French government operated by the National Research Agency (ANR). TG acknowledges support from an Australian Research Council SuperScience Fellowship. The authors thank Léo Michel-Dansac for the  $N$ -body simulation used in this study. This work was granted access to the HPC resources of CINES under the allocation 2012-c2012046642 made by GENCI (Grand Equipement National de Calcul Intensif).

## REFERENCES

- Bacon R. et al., 2006, *The Messenger*, 124, 5  
 Bacon R. et al., 2010, *Proc. SPIE*, 7735, 773508  
 Barnes L. A., Garel T., Kacprzak G. G., 2014, *PASP*, 126, 969  
 Battaglia G. et al., 2005, *MNRAS*, 364, 433  
 Birnboim Y., Dekel A., 2003, *MNRAS*, 345, 349  
 Blaizot J., Guiderdoni B., Devriendt J. E. G., Bouchet F. R., Hatton S. J., Stoehr F., 2004, *MNRAS*, 352, 571  
 Blaizot J., Wadadekar Y., Guiderdoni B., Colombi S. T., Bertin E., Bouchet F. R., Devriendt J. E. G., Hatton S., 2005, *MNRAS*, 360, 159  
 Blanc G. A. et al., 2011, *ApJ*, 736, 31  
 Bouwens R. J., Illingworth G. D., Franx M., Ford H., 2007, *ApJ*, 670, 928  
 Bouwens R. J. et al., 2009, *ApJ*, 705, 936  
 Bouwens R. J. et al., 2015, *ApJ*, 803, 34  
 Caputi K. I., Cirasuolo M., Dunlop J. S., McLure R. J., Farrah D., Almaini O., 2011, *MNRAS*, 413, 162  
 Cassata P. et al., 2011, *A&A*, 525, A143  
 Cattaneo A., Dekel A., Devriendt J., Guiderdoni B., Blaizot J., 2006, *MNRAS*, 370, 1651  
 Davis M., Efstathiou G., Frenk C. S., White S. D. M., 1985, *ApJ*, 292, 371  
 Dayal P., Libeskind N. I., 2012, *MNRAS*, 419, L9  
 Dayal P., Ferrara A., Gallerani S., 2008, *MNRAS*, 389, 1683  
 Dayal P., Ferrara A., Saro A., 2010, *MNRAS*, 402, 1449  
 Dayal P., Maselli A., Ferrara A., 2011, *MNRAS*, 410, 830  
 Dekel A. et al., 2009, *Nature*, 457, 451  
 Devriendt J. E. G., Guiderdoni B., Sadat R., 1999, *A&A*, 350, 381  
 Dijkstra M., Lidz A., Wyithe J. S. B., 2007, *MNRAS*, 377, 1175  
 Dijkstra M., Mesinger A., Wyithe J. S. B., 2011, *MNRAS*, 414, 2139  
 Domínguez Sánchez H. et al., 2011, *MNRAS*, 417, 900  
 Dressler A., Martin C. L., Henry A., Sawicki M., McCarthy P., 2011, *ApJ*, 740, 71  
 Dressler A., Henry A., Martin C. L., Sawicki M., McCarthy P., Villaneuva E., 2015, *ApJ*, 806, 19  
 Duncan K. et al., 2014, *MNRAS*, 444, 2960  
 Efstathiou G., 1992, *MNRAS*, 256, 43p  
 Elsner F., Feulner G., Hopp U., 2008, *A&A*, 477, 503  
 Fontana A. et al., 2006, *A&A*, 459, 745  
 Forero-Romero J. E., Yepes G., Gottlöber S., Knollmann S. R., Cuesta A. J., Prada F., 2011, *MNRAS*, 415, 3666  
 Furlanetto S. R., Zaldarriaga M., Hernquist L., 2006, *MNRAS*, 365, 1012  
 Garel T., Blaizot J., Guiderdoni B., Schaerer D., Verhamme A., Hayes M., 2012, *MNRAS*, 422, 310  
 Garel T., Blaizot J., Guiderdoni B., Michel-Dansac L., Hayes M., Verhamme A., 2015, *MNRAS*, 450, 1279  
 Gawiser E. et al., 2007, *ApJ*, 671, 278  
 González V., Labbé I., Bouwens R. J., Illingworth G., Franx M., Kriek M., 2011, *ApJ*, 735, L34  
 González J. E., Lacey C. G., Baugh C. M., Frenk C. S., Benson A. J., 2012, *MNRAS*, 423, 3709  
 Gronwall C. et al., 2007, *ApJ*, 667, 79  
 Haiman Z., Spaans M., 1999, *ApJ*, 518, 138  
 Hatton S., Devriendt J. E. G., Ninin S., Bouchet F. R., Guiderdoni B., Vibert D., 2003, *MNRAS*, 343, 75  
 Hayashino T. et al., 2004, *AJ*, 128, 2073  
 Hill G. J. et al., 2008, in Kodama T., Yamada T., Aoki K., eds, *ASP Conf. Ser. Vol. 399, Panoramic Views of Galaxy Formation and Evolution*. Astron. Soc. Pac., San Francisco, p. 115  
 Hu E. M., Cowie L. L., McMahon R. G., 1998, *ApJ*, 502, L99  
 Hu E. M., Cowie L. L., Barger A. J., Capak P., Kakazu Y., Trouille L., 2010, *ApJ*, 725, 394  
 Hutter A., Dayal P., Müller V., 2015, *MNRAS*, 450, 4025  
 Iliev I. T., Shapiro P. R., McDonald P., Mellema G., Pen U.-L., 2008, *MNRAS*, 391, 63  
 Inoue A. K., Shimizu I., Iwata I., Tanaka M., 2014, *MNRAS*, 442, 1805  
 Jensen H., Laursen P., Mellema G., Iliev I. T., Sommer-Larsen J., Shapiro P. R., 2013, *MNRAS*, 428, 1366  
 Jose C., Srianand R., Subramanian K., 2013, *MNRAS*, 435, 368  
 Kaffle P. R., Sharma S., Lewis G. F., Bland-Hawthorn J., 2014, *ApJ*, 794, 59  
 Kajisawa M. et al., 2009, *ApJ*, 702, 1393  
 Kajisawa M., Ichikawa T., Yamada T., Uchimoto Y. K., Yoshikawa T., Akiyama M., Onodera M., 2010, *ApJ*, 723, 129  
 Kashikawa N. et al., 2011, *ApJ*, 734, 119  
 Kennicutt R. C., Jr, 1983, *ApJ*, 272, 54  
 Kennicutt R. C., Jr, 1998, *ApJ*, 498, 541  
 Kobayashi M. A. R., Totani T., Nagashima M., 2007, *ApJ*, 670, 919  
 Kobayashi M. A. R., Totani T., Nagashima M., 2010, *ApJ*, 708, 1119

- Komatsu E. et al., 2009, *ApJS*, 180, 330
- Kovač K., Somerville R. S., Rhoads J. E., Malhotra S., Wang J., 2007, *ApJ*, 668, 15
- Kudritzki R. et al., 2000, *ApJ*, 536, 19
- Kunth D., Mas-Hesse J. M., Terlevich E., Terlevich R., Lequeux J., Fall S. M., 1998, *A&A*, 334, 11
- Lanzoni B., Guiderdoni B., Mamon G. A., Devriendt J., Hatton S., 2005, *MNRAS*, 361, 369
- Laursen P., Sommer-Larsen J., Andersen A. C., 2009, *ApJ*, 704, 1640
- Laursen P., Sommer-Larsen J., Razoumov A. O., 2011, *ApJ*, 728, 52
- Le Delliou M., Lacey C., Baugh C. M., Guiderdoni B., Bacon R., Courtois H., Sousbie T., Morris S. L., 2005, *MNRAS*, 357, L11
- Le Fèvre O. et al., 2015, *A&A*, 576, A79
- McLinden E., Finkelstein S. L., Rhoads J. E., Malhotra S., Hibon P., Richardson M., 2011, *AAS Meeting # 217*, 335.43
- McMillan P. J., 2011, *MNRAS*, 414, 2446
- McQuinn M., Hernquist L., Zaldarriaga M., Dutta S., 2007, *MNRAS*, 381, 75
- McQuinn M., Lidz A., Zahn O., Dutta S., Hernquist L., Zaldarriaga M., 2007, *MNRAS*, 377, 1043
- Madau P., 1995, *ApJ*, 441, 18
- Malhotra S., Rhoads J. E., 2004, *ApJ*, 617, L5
- Mandelbaum R., Seljak U., Kauffmann G., Hirata C. M., Brinkmann J., 2006, *MNRAS*, 368, 715
- Marchesini D., van Dokkum P. G., Förster Schreiber N. M., Franx M., Labbé I., Wuyts S., 2009, *ApJ*, 701, 1765
- Mas-Hesse J. M., Kunth D., Tenorio-Tagle G., Leitherer C., Terlevich R. J., Terlevich E., 2003, *ApJ*, 598, 858
- Moster B. P., Somerville R. S., Newman J. A., Rix H.-W., 2011, *ApJ*, 731, 113
- Murayama T. et al., 2007, *ApJS*, 172, 523
- Nagamine K., Ouchi M., Springel V., Hernquist L., 2010, *PASJ*, 62, 1455
- Nakamura E., Inoue A. K., Hayashino T., Horie M., Kousai K., Fujii T., Matsuda Y., 2011, *MNRAS*, 412, 2579
- Neufeld D. A., 1990, *ApJ*, 350, 216
- Ocvirk P., Pichon C., Teyssier R., 2008, *MNRAS*, 390, 1326
- Okamoto T., Gao L., Theuns T., 2008, *MNRAS*, 390, 920
- Orsi A., Lacey C. G., Baugh C. M., 2012, *MNRAS*, 425, 87
- Osterbrock D. E., Ferland G. J., 2006, *Astrophysics of Gaseous Nebulae and Active Galactic Nuclei*. University Science Books, Sausalito, CA
- Ouchi M. et al., 2003, *ApJ*, 582, 60
- Ouchi M. et al., 2008, *ApJS*, 176, 301
- Ouchi M. et al., 2010, *ApJ*, 723, 869
- Pentericci L., Grazian A., Fontana A., Salimbeni S., Santini P., de Santis C., Gallozzi S., Giallongo E., 2007, *A&A*, 471, 433
- Pérez-González P. G. et al., 2008, *ApJ*, 675, 234
- Phelps S., Nusser A., Desjacques V., 2013, *ApJ*, 775, 102
- Rauch M. et al., 2008, *ApJ*, 681, 856
- Reddy N. A., Steidel C. C., Pettini M., Adelberger K. L., Shapley A. E., Erb D. K., Dickinson M., 2008, *ApJS*, 175, 48
- Rhoads J. E., Malhotra S., Dey A., Stern D., Spinrad H., Jannuzi B. T., 2000, *ApJ*, 545, L85
- Rivera-Thorsen T. E. et al., 2015, *ApJ*, 805, 14
- Salmon B. et al., 2015, *ApJ*, 799, 183
- Salvadori S., Dayal P., Ferrara A., 2010, *MNRAS*, 407, L1
- Santos M. R., 2004, *MNRAS*, 349, 1137
- Sawicki M., Thompson D., 2006, *ApJ*, 648, 299
- Sawicki M. et al., 2008, *ApJ*, 687, 884
- Schaerer D., Hayes M., Verhamme A., Teyssier R., 2011, *A&A*, 531, A12
- Schaerer D., de Barros S., Sklias P., 2013, *A&A*, 549, A4
- Shapley A. E., Steidel C. C., Adelberger K. L., Dickinson M., Giavalisco M., Pettini M., 2001, *ApJ*, 562, 95
- Shapley A. E., Steidel C. C., Pettini M., Adelberger K. L., 2003, *ApJ*, 588, 65
- Shimasaku K. et al., 2006, *PASJ*, 58, 313
- Shimizu I., Yoshida N., Okamoto T., 2011, *MNRAS*, 418, 2273
- Shioya Y. et al., 2009, *ApJ*, 696, 546
- Silk J., 2003, *MNRAS*, 343, 249
- Song M. et al., 2015, preprint ([arXiv:1507.05636](https://arxiv.org/abs/1507.05636))
- Springel V., 2005, *MNRAS*, 364, 1105
- Stark D. P., Schenker M. A., Ellis R., Robertson B., McLure R., Dunlop J., 2013, *ApJ*, 763, 129
- Steidel C. C., Erb D. K., Shapley A. E., Pettini M., Reddy N., Bogosavljević M., Rudie G. C., Rakic O., 2010, *ApJ*, 717, 289
- Tenorio-Tagle G., Silich S. A., Kunth D., Terlevich E., Terlevich R., 1999, *MNRAS*, 309, 332
- Tweed D., Devriendt J., Blaizot J., Colombi S., Slyz A., 2009, *A&A*, 506, 647
- van Breukelen C., Jarvis M. J., Venemans B. P., 2005, *MNRAS*, 359, 895
- van den Bosch F. C., Yang X., Mo H. J., 2003, *MNRAS*, 340, 771
- van der Burg R. F. J., Hildebrandt H., Erben T., 2010, *A&A*, 523, A74
- Verhamme A., Schaefer D., Maselli A., 2006, *A&A*, 460, 397
- Verhamme A., Schaefer D., Atek H., Tapken C., 2008, *A&A*, 491, 89
- Verhamme A., Dubois Y., Blaizot J., Garel T., Bacon R., Devriendt J., Guiderdoni B., Slyz A., 2012, *A&A*, 546, A111
- Walker-Soler J. P., Gawiser E., Bond N. A., Padilla N., Francke H., 2012, *ApJ*, 752, 160
- Wilkins S. M., Gonzalez-Perez V., Lacey C. G., Baugh C. M., 2012, *MNRAS*, 427, 1490
- Wofford A., Leitherer C., Salzer J., 2013, *ApJ*, 765, 118
- Yajima H., Li Y., Zhu Q., Abel T., 2012a, *MNRAS*, 424, 884
- Yajima H., Li Y., Zhu Q., Abel T., Gronwall C., Ciardullo R., 2012b, *ApJ*, 754, 118
- Yamada T., Nakamura Y., Matsuda Y., Hayashino T., Yamauchi R., Morimoto N., Kousai K., Umemura M., 2012, *AJ*, 143, 79
- Yang X., Mo H. J., van den Bosch F. C., 2009, *ApJ*, 695, 900
- Zheng Z., Cen R., Trac H., Miralda-Escudé J., 2010, *ApJ*, 716, 574

This paper has been typeset from a  $\text{\TeX}/\text{\LaTeX}$  file prepared by the author.